MIT Libraries | DSpace@MIT

MIT Open Access Articles

Alternative Splicing of FN (Fibronectin) Regulates the Composition of the Arterial Wall Under Low Flow

The MIT Faculty has made this article openly available. ***Please share*** how this access benefits you. Your story matters.

Citation: Murphy, Patrick A. et al. "Alternative Splicing of FN (Fibronectin) Regulates the Composition of the Arterial Wall Under Low Flow." Arteriosclerosis, Thrombosis, and Vascular Biology 41, 1 (November 2020): e18–e32. © 2020 Lippincott Williams and Wilkins

As Published: http://dx.doi.org/10.1161/atvbaha.120.314013

Publisher: Ovid Technologies (Wolters Kluwer Health)

Persistent URL: https://hdl.handle.net/1721.1/131166

Version: Author's final manuscript: final author's manuscript post peer review, without publisher's formatting or copy editing

Terms of use: Creative Commons Attribution-Noncommercial-Share Alike

Massachusetts Institute of Technology

Alternative Splicing of Fibronectin Regulates the Composition of the Arterial Wall Under Low Flow

Patrick A. Murphy[1,2,*], Noor Jailkhani[1], Sarah-Anne Nicholas[2], Amanda M. Del Rosario[1], Jeremy L. Balsbaugh[3], Shahinoor Begum[1,4], Amy Kimble[2], Richard O. Hynes[1,4],*

1 Koch Institute for Integrative Cancer Research, MIT, Cambridge, MA 02139
2 UCONN Health, Farmington, CT 06030
3 UCONN, Proteomics and Metabolomics Facility, Storrs, CT 06269
4 Howard Hughes Medical Institute, Chevy Chase, MD 20815

* Co-corresponding authors

Correspondence

Patrick Murphy
Email: pamurphy@uchc.edu

Richard Hynes
Email: rohynes@mit.edu

Objective:
Exposure of the arterial endothelium to low and disturbed flow is a risk factor for the erosion and rupture of atherosclerotic plaques and aneurysms. Circulating and locally produced proteins are known to contribute to an altered composition of the extracellular matrix (ECM) at the site of lesions, and to contribute to inflammatory processes within the lesions. We have previously shown that alternative splicing of fibronectin (FN) protects against flow-induced hemorrhage. However, the impact of alternative splicing of FN on ECM composition remains unknown.
Approach and Results:
Here, we perform quantitative proteomic analysis of the matrisome of murine carotid arteries in mice deficient in the production of FN splice isoforms containing alternative exons EIIIA and EIIIB (FN-EIIIAB null) after exposure to low and disturbed flow *in vivo.* We also examine serum-derived and endothelial-cell contributions to the matrisome in a simplified *in vitro* system. We found flow-induced differences in the carotid artery matrisome that were impaired in FN-EIIIAB null mice. One of the most interesting differences was reduced recruitment of fibulin-1 (FBLN1), abundant in blood and not locally produced in the intima. This defect was validated in our *in vitro* assay, where FBLN1 recruitment from serum was impaired by the absence of these alternatively spliced segments.
Conclusions:
Our results reveal the extent of the dynamic alterations in the matrisome in the acute response to low and disturbed flow, and show how changes in the splicing of FN, a common response in vascular inflammation and remodeling, can affect matrix composition. (247 words)

Introduction:

Low and disturbed flow is an initiating event in the formation of atherosclerotic lesions [1-3], and is linked to the symptomatic progression of atherosclerotic plaque [4]. The endothelial lining of arteries responds directly to low flow, leading to altered signaling and increased recruitment of blood cells [3]. Disease progression is driven by changes in the extracellular matrix resembling the response to vascular injury [5]. Fibronectin (FN) is a critical component of the provisional matrix deposited at sites of injury in the vasculature and elsewhere [6]. Increased fibronectin (FN) in the sub-endothelial matrix is among the earliest changes at arterial branch points predisposed to atherosclerotic lesion formation by low and disturbed flow [7]. While some of this is locally produced, a large portion of this protein is derived from circulating FN in the blood [8]. FN and other matrix proteins can contribute directly to atherosclerosis progression by promoting endothelial activation [7] and trapping plasma proteins in the arterial wall as they are driven in by pressure gradients [9]. Fibulin1 (FBLN1) is also strongly recruited to atherosclerotic lesions. FBLN1, like FN, is abundant in blood [10], and reduced FBLN1 levels in circulation are correlated with early-onset atherosclerosis [11]. While the changes in a few matrisome proteins, like FN, have been identified early in the response to low flow, the matrisome response to low flow has not been broadly assessed, and it is not clear whether other circulating proteins, like FBLN1 are also recruited to the activated arterial wall.

Recently, we demonstrated that recruitment of innate immune cells under low flow acutely alters endothelial RNA splicing patterns in FN in the arterial endothelium, and that these locally produced splice variants are protective against hemorrhagic rupture of the intima [12]. As one of the first matrix proteins deposited at the site of injury, FN determines the subsequent matrisome deposition of other proteins including collagens, fibrillins, fibulins, latent TGF-β binding protein (LTBP), tenascin-C and proteoglycans [6]. Splice isoforms of FN including the alternative exons EIIIA and EIIIB are upregulated in early vascular development and angiogenesis, and also in pathologic

responses involving vascular remodeling, such as atherosclerosis, aneurysms, lung and liver fibrosis, wound healing and cancer [13], suggesting that the inclusion of these domains may have a fundamentally important role in the remodeling of the extracellular matrix around the vasculature. Despite their potential to modify matrisome organization, the impact of FN spliced domains on the composition of the vascular matrisome has not been examined.

Here, we examine the response of the arterial matrisome to low flow, and the effect of altered FN splicing on this response *in vivo* and in an *in vitro* model. We find that the levels of FBLN1 and several other proteins with roles in human vascular disease and development are modulated by the expression of FN splice variants.

Methods:

Data and unique reagents have been made available. All proteomics data have been made publicly available at the ProteomeXchange Consortium via the PRIDE [14] partner repository with the dataset identifier PXD012474 and 10.6019/PXD012474. Mouse line (*FnAB-null*) is available from JAX, as strain *B6;129P2-Fn1tm4Hyn/J* (Stock 008595). Cell lines generated from these mice that support the findings of this study are available from the corresponding author upon reasonable request.

Partial carotid ligation model of low and disturbed flow

Partial carotid ligations were performed as previously described [15], with minor modifications [12]. Briefly, the distal branches of the left carotid artery were identified in mice anesthetized with isoflurane. The left external carotid, internal carotid, and occipital artery were ligated with 9-0 Ethilon sutures, leaving only the superior thyroid artery intact. Sham operations consisted of the same carotid dissection and encircling with suture, except that the vessels were not tied off. High-resolution ultrasound, using the VisualSonics Vevo 770, was performed at the experimental endpoint (2-7 days after partial carotid ligation) to confirm vessel patency.

All mice were housed and handled in accordance with IACUC approved protocols in accordance with the Massachusetts Institute of Technology Division of Comparative Medicine and the University of Connecticut Health Center for Comparative Medicine.

In vitro culture of aortic endothelial cells

Mouse aortic endothelial cells were isolated from 3 pairs of littermate *FnAB-null* and *FnAB-het* mice following previously described methods [16], with modifications. Briefly, mice were perfused via the left ventricle with PBS, the aorta was isolated and filled with 2% collagenase II (Worthington) in serum-free DMEM, and then closed at the ends with 7-0 suture. The vessel was digested for 30-45 minutes in 10%FBS at 37C, and endothelial cells were flushed out into EC culture media, and onto a collagen I-coated plate. EC culture medium consisted of DMEM with 10% FBS and 10mg/mL endothelial growth supplement (ECGS, Biomedical Technologies) with primocin (InVivogen). Typical isolations of ~1000 cells expanded to ~10,000-50,000 cells. Cells were then FACs-sorted (BD Aria) on endothelial markers; FITC acetylated-Ldl+, Pecam+ and Icam2+.

After purification by FACs, endothelial cells were immortalized by lentiviral TetOn-Sv40T antigen. The construct was developed from a version of pTripz [17] with removal of the puro selection cassette. SV40T was inserted into the tet-regulated region of the lentivirus from pBabe-SV40 [18]. After infection, cells were expanded in EC media with 2ug/mL doxycycline (Dox).

For the preparation of endothelial matrix *in vitro*, early-passage aortic endothelial cells were trypsinized and 2x10^5 cells were plated in 10cm dishes in 5% biotin-labeled human serum. Serum had been biotin labeled (2hrs at 37C in a glass tube) at 1.5 molar ratio of biotin:protein (for proteins with 50kDa mass), and then dialyzed overnight in 2kDa membrane. SV40T was turned off, since media did not contain Dox. After 15 days, an additional 1mL of 5% biotin-labeled human serum was added to each plate, and cells were harvested 8hrs later.

Extracellular matrix purification from cells

Medium was collected. Cells were washed 4x in PBS with 1mM Mg++ and Ca++, collecting the last wash. 1mL of 1% DOC in 20mM Tris pH 8.5 was added, cells and matrix were scraped from the plate, and snap frozen.

Samples were thawed on ice, and 1uL of Benzonase (Sigma) was added to each 1mL tube to digest nucleic acids. After incubating for 15 min at 37C, samples were spun down at 12,000 rcf at 4C. The 1% DOC soluble supernatant was removed, and the pellet was sequentially washed with 1mL of 1% DOC 20mM Tris pH 8.5 and 1mL 50mM ammonium bicarbonate, saving the supernatant from each step. The final pellet was left in 100uL 8M urea ammonium bicarbonate with DTT for later digestion.

For capture of proteins from the 1% DOC-soluble fraction, 200uL of each of two 1% DOC soluble supernatants were added to 1.6mL PBS (for a final 0.2% DOC concentration). 100uL of Neutravidin beads were added and incubated at 4C for 1hr. Beads were washed sequentially with 1mL 1% DOC with 20mM Tris, and 2x 1mL 50mM ammonium bicarbonate with 2500g spins between washes, before resuspending in 100uL 8M urea ammonium bicarbonate with DTT for digestion.

Digestion of pellet and biotin-pull-down from the 1% DOC-soluble fraction was performed generally following the protocol described by Naba et al. [19]. Briefly, samples were reduced with DTT and alkylated with iodoacetamide in 8M Urea. They were PNGase-treated in 2M Urea and then digested with LysC and then Trypsin. Digestion was stopped with 0.1% trifluroacetic acid (TFA) and the peptides were then cleaned up on a C18 reverse-phase column. Cartridges were washed with 3 mL of acetonitrile, 3 mL of 0.5% acetic acid, 50% acetonitrile in water, and 3 mL of 0.1% TFA in water. After loading the peptide mixtures, the cartridges were washed with 3 mL of 0.1% TFA and then with 0.250 mL of 0.5% acetic acid in water. The peptides were eluted with 1 mL of 0.5% acetic acid, 80% acetonitrile in water, and dried in a Speed Vac (Thermo).

In addition to the analysis of cells and associated proteins bound from serum, the serum used was analyzed directly in parallel. Serum was added to 100uL 8M urea ammonium bicarbonate with DTT for digest, PNGase-treated in 2M Urea and then digested with LysC and then Trypsin. Digestion was stopped with 0.1% trifluroacetic acid (TFA) and the peptides were then cleaned up on a C18 reverse-phase column.

Extracellular matrix enrichment from carotid arteries

in situ biotinylation. At the time of harvest, the vasculature was perfused with 20mL PBS through the left ventricle immediately following euthanasia. This was followed by perfusion with ice-cold 0.5mg/mL Sulfo-NHS-LC-Biotin in PBS, compressing the descending aorta to selectively perfuse upper vasculature. This was left in place for 5min on ice, before stopping by perfusion of 10mL of 100mM glycine. Carotids were then dissected, and flushed again with 100mM glycine with an insulin syringe, and snap frozen.

Carotids from FnAB-het and -null mice were pooled (3 carotids for each group). The ECM was enriched using the CNMCS Compartment Protein Extraction Kit (EMD Millipore, MA) by the sequential extraction of Cytoplasmic, Nuclear, Membrane and Cytoskeletal proteins. The manufacturers' protocol was optimized for the small sample amount. Briefly, the pooled carotids were homogenized in a bullet blender (Next Advance, NY) using SSB14B (0.9-2mm stainless steel beads) in 45 µl of Buffer C with protease inhibitor and benzonase, rotated for 20 minutes at 4°C and then spun at 4°C for 30 minutes at 13,000g. The supernatant was collected as fraction 1 (Cytoplasmic protein fraction). The pellet was washed with 25 µl of Buffer W and re-suspended in 20 µl of Buffer N, pipet-mixed periodically for 30 minutes at 4°C and spun for 20 minutes at 13,000g. The supernatant was collected as fraction 2 (Nuclear protein fraction). The pellet was again washed with 25 µl buffer W and re-suspended in 10 µl of Buffer M, pipet mixed periodically for 30 minutes at 4°C and spun for 30 minutes at 13,000g. The supernatant was collected as fraction 3 (Membrane protein fraction) and the pellet was finally re-suspended in 10 µl of Buffer CS with benzonase, incubated at room temperature with periodic pipet-mixing for 15 minutes, spun for 30 minutes at 13,000g and the collected supernatant was saved as Fraction 4 (Cytoskeletal protein fraction). The final ECM-enriched insoluble pellet was re-suspended in 12.5 µl of Buffer C, rotated for 15 minutes at 4°C, spun for 20 minutes at 13,000g and the supernatant was stored as Fraction 5 (Cytoplasmic wash fraction). The ECM enrichment was confirmed by western blotting. The final ECM-enriched pellet was solubilized and digested for Mass Spectrometry using protocols previously described [19].

Soluble extracellular proteins lost during the enrichment of insoluble matrix were collected by Neutravidin bead pulldown. Fractions 1-5 and intervening washes were combined and brought to 1mL in PBS. They were incubated for 30min at 4C with 100uL neutravidin beads (Thermo), and then spun at 4°C for 1 minute at 2,500g. The supernatant was removed and bead-bound biotin proteins were washed twice with 1mL of 1%DOC to remove cell-derived DOC-soluble proteins without the biotin tag, then 1mL PBS, and then twice with 50mM ammonium bicarbonate. Digestion of bound and biotinylated proteins were performed on the beads, by suspending the beads and digesting according to published protocols [19].

Quantitative mass spectrometry – In Vivo Soluble and Insoluble fractions

Sample preparation

Following carbamidomethylation and trypsinization, all peptides were desalted using Pierce C18 spin columns (Thermo Scientific, P/N 89870) according to manufacturer's instructions. Dried, desalted peptides were resuspended in 100 µL 100 mM triethylammonium bicarbonate (TEAB) and labeled using the TMT10plex mass tag labeling kit (Thermo Scientific) and manufacturer's instructions. Following TMT labeling, all samples were desalted using methods previously described. A small aliquot of each TMT-labeled peptide sample was analyzed using LCMS to verify labeling efficiency using the MaxQuant software package [20] as previously described in [21]. TMT-labeled samples were mixed at equal peptide amounts as determined by A280 absorbance using a Nanodrop spectrophotometer (Thermo Scientific). A screening LCMS analysis of the pooled sample was used to determine the mixing accuracy for all 10 TMT channels using Sequest HT and Proteome Discoverer (v2.2, Thermo Scientific) using search parameters listed for the main peptide and protein identification and quantitation searches as described in detail below. Mixing accuracy was determined by calculating the median ratio for all peptide intensities in each TMT channel over the corresponding peptide intensity in the control sample. In cases where enough material allowed, these correction factors were used to fine-tune the mixing accuracy to yield a median ratio as close as possible to 1.00.

Once samples were optimally mixed, soluble and insoluble samples were subjected to fractionation using Pierce high pH reversed-phase peptide fractionation columns (Thermo Scientific, P/N 84868) according to manufacturer's instruction for TMT-labeled peptides. Both sample sets were fractionated into 8 elution fractions plus a high pH (0.1% triethylamine) wash fraction. Each fraction was dried, resuspended in 0.1% formic acid in water and quantified by A280 absorbance. Fractions were then condensed into 6 total mixtures for LCMS analysis as follows: 0.1% triethylamine wash fraction, fraction 1, fraction 2+5, fraction 3+6, fraction 4+7, fraction 8.

LCMS analysis details

All 6 fractions were reconstituted in 0.1% formic acid in water to yield a final injection peptide concentration of 100 ng/µL and analyzed using an UltiMate 3000 RSLCnano liquid chromatography system coupled directly to a Q Exactive HF Orbitrap mass spectrometer (Thermo Scientific). The UltiMate 3000 RSLCnano was operated in direct injection mode with a 50°C continuous column oven temperature. Peptides were separated using a 300 nL/min flow rate, nanoEase m/z peptide analytical BEH C18 column (180Å pore size, 1.7 µm particle size, P/N 186008795, Waters Corp) and linear gradient using solvent A (0.1% formic acid in water) and B (0.1% formic acid in acetonitrile) as follows: 4% B (0-10 min), 4-30% B (10-150 min), 30-90% (150-180 min), 90% hold (180-190 min), 90-4% B (190-192 min), 4% B (192-210 min). The Q Exactive HF was operated in positive mode with a 2.5 kV capillary voltage. A 210 min top 15 data-dependent MS/MS (ddMS/MS) method was implemented to acquire in profile mode with the following parameters for MS1 scans: 120,000 resolution, 300 to 1400 m/z scan range, 1e6 AGC target, 50 ms maximum injection time, and 1 microscan per spectrum. All ddMS/MS scans were acquired using the following settings: 60,000 resolution, fixed first mass of 100.0 m/z, 1e5 AGC target, 100 ms maximum injection time, 0.7 m/z isolation window, unassigned, +1, +8, and >+8 charge state exclusion, "preferred" peptide match, dynamic exclusion window of 30 s, 0.0 m/z isolation offset, 33 normalized collision energy, exclude isotopes "on," and 1 microscan per spectrum.

Data analysis details

Sequest HT and Proteome Discoverer (v2.2, Thermo Scientific) were used to identify TMT-labeled peptides and perform protein-level quantitation using TMT reporter-ion intensities. For fractionated samples, all 6 .raw files were loaded and searched simultaneously against the Uniprot *Mus musculus* reference proteome database (Accessed May 16 2017) using the following parameters: trypsin enzyme specificity with 2 maximum missed cleavages, minimum and maximum peptide lengths of 6 and 144, respectively, static modifications of TMT6plex on peptide N-termini and Lys plus carbamidomethylation on Cys, dynamic modifications of oxidation on Met and Pro, deamidation on Asn, plus protein N-terminal acetylation, precursor and fragment mass tolerances of 5 ppm and 0.02 Da, respectively,. All data were filtered to a strict 1% FDR at the PSM, peptide and protein levels. Quantification was performed on unique and razor peptides, quantification values were corrected based on the manufacturer's isotope purity report. The ratio calculation was based on the summed abundance of peptides (e.g. intensity of all peptides of protein A labeled with TMT label 1 were combined and then compared with the similar combinations from TMT label 2, label 3, label 4, etc). Razor-peptides are non-unique peptides, which are assigned to their associated protein group containing the largest number of other peptides. All other parameters were kept at software defaults. Matrisome proteins were determined as previously defined [22].

Quantitative mass spectrometry – *in vitro* Co-culture

Peptide labeling with TMT 10plex (Thermo) was performed per manufacturer's instructions. Lyophilized samples were dissolved in 70 µL ethanol and 30 µL of 500 mM triethylammonium bicarbonate, pH 8.5, and the TMT reagent was dissolved in 30 µL of anhydrous acetonitrile. The

273 solution containing peptides and TMT reagent was vortexed and incubated at room temperature
274 for 1 h. Samples labeled with the ten different isotopic TMT reagents were combined and
275 concentrated to minimal volume in a vacuum centrifuge.
276
277 The TMT-labeled peptide pellet was fractioned via high-pH reversed-phase HPLC. Peptides were
278 resuspended in 100uL buffer A (10mM TEAB, pH8) and separated on a 4.6mm x 250 mm
279 300Extend-C18, 5um column (Agilent) using a 90 minute gradient with buffer B (90% MeCN,
280 10mM TEAB, pH8) at a flow rate of 1ml/min. The gradient was as follows: 1-5% B (0-10min), 5-
281 35% B (10-70min), 35-70% B (70-80min), 70% B (80-90min). Fractions were collected over 75
282 minutes at 1 minute intervals from 10 min to 85 min. The fractions were concatenated into 15
283 fractions non-contiguously (1+16+31+46+61, 2+17+32+47+62, etc). The fractions were
284 concentrated by Speed-Vac (Thermo Scientific Savant) to near dryness.
285
286 The 15 different peptide fractions were loaded on a precolumn and separated by reversed-phase
287 HPLC using an EASY- nLC1000 (Thermo) over a 140 minute gradient before nanoelectrospray
288 using a QExactive Plus mass spectrometer (Thermo). The mass spectrometer was operated in a
289 data-dependent mode. The parameters for the full-scan MS were: resolution of 70,000 across 350-
290 2000 *m/z*, AGC $3e^6$, and maximum IT 50 ms. The full MS scan was followed by MS/MS for the top
291 10 precursor ions in each cycle with a NCE of 34 and dynamic exclusion of 30 s. Raw mass-
292 spectral data files (.raw) were searched using Proteome Discoverer (Thermo) and Mascot version
293 2.4.1 (Matrix Science). Mascot search parameters were: 10 ppm mass tolerance for precursor
294 ions; 15 mmu for fragment ion mass tolerance; 2 missed cleavages of trypsin; fixed modifications
295 were carbamidomethylation of cysteine and TMT 10plex modification of lysines and peptide N-
296 termini; variable modifications were oxidized methionine, deamidation of asparagine, pyro-glutamic
297 acid modification at N-terminal glutamine, and hydroxylation of proline. TMT quantification was
298 obtained using Proteome Discoverer and isotopically corrected per manufacturer's instructions,
299 and normalized to the mean of each TMT channel. Only peptides with a Mascot score greater than
300 or equal to 25 and an isolation interference less than or equal to 30 were included in the data
301 analysis. Matrisome proteins were determined as previously defined [22]. The mass spectrometry
302 proteomics data have been deposited to the ProteomeXchange Consortium via the PRIDE [14]
303 partner repository with the dataset identifier PXD012474 and 10.6019/PXD012474.
304
305 **Immunofluorescence**
306 Cultured cells were removed from Dox (to turn off SV40) and plated on acid-washed glass
307 coverslips precoated with Collagen I (Rat Tail, Thermo A1048301). They were cultured in the
308 presence of 10% human serum in DMEM (Innovative Research Inc, IPLA-SER) for the indicated
309 number of days, and then fixed briefly in 4% paraformaldehyde in PBS on ice. After washing, they
310 were blocked and stained for Fibulin-1 (Abcam, ab211536) and Fibronectin (293.1 a rabbit
311 polyclonal and a gift from the Richard Hynes Lab), followed by anti-mouse 594 and anti-rabbit 488.
312
313 **Western Blots**
314 Protein samples were reduced and denatured and separated on a Tris-glycine SDS-PAGE gel
315 before transfer to Immobilon-P PVDF Membrane (Sigma IPVH00010). Membranes were blocked in
316 5% Dry milk in TBS-T, and then incubated with Fibulin-1 (Abcam, ab211536) and then Fibronectin
317 (293.1 a rabbit polyclonal and a gift from the Richard Hynes Lab), followed by anti-mouse or anti-
318 rabbit HRP-conjugated secondary antibodies ().
319
320 **Statistical analysis of proteins differentially enriched in matrix fraction of *FnAB-null* vs**
321 ***FnAB-het* mice**

Prior to comparisons, peptides not found in each TMT channel were trimmed. Data analysis was performed from spectral intensity files, following quantile normalization using Limma. Limma is a statistical approach which was developed for microarray data, which uses an estimated variance to overcome the problem of irregular variances from a small N in quantitative proteomics experiments [23]. Quantile normalization further smooths quantitative proteomics data by adjusting each data set so that the variance~~s~~ within each TMT channel is set to be equivalent with other channels, resulting in a further increase in ability to detect real differences at the same false-detection rate [24, 25]. Unless otherwise stated, unadjusted, nominal P-values are presented. Benjamini-Hochberg FDR levels are provided as supplementary material.

Results:

Analysis of alterations in matrisome composition in the acute response to disturbed flow

We isolated enriched extracellular matrix (see Methods) from the carotid arteries of C57BL6/J background *Fn-EIIIAB-/-* and *Fn-EIIIAB+/-* mice (hereafter *FnAB-null* and *FnAB-het*) 7 days after exposure to low flow through partial carotid ligation (Figure 1A). This is a timepoint corresponding to the end of an acute process in the low-flow artery involving both inward remodeling, neointima formation, and cell proliferation [26]. As we have previously observed, defects in FN splicing resulted in a partially penetrant hemorrhagic phenotype (5/9 in *FnAB-null* and 5/10 in *FnAB-het* (SI Figure 1, [12]). In parallel experiments, 0/12 age-matched C57BL6/J wild-type mice displayed this hemorrhagic phenotype (SI Figure 1). These data suggest the possibility that even a partial loss of FN splicing function may increase the risk of arterial hemorrhage. Comparisons between *FnAB-null* and WT mice would show combined changes due both to hemorrhage and to loss of the splice segments, without separating them. Accordingly, we pooled vessels from *FnAB-null* and *FnAB-het* mice, with similar mixes of mild and severe hemorrhagic phenotypes, to focus on detection solely of changes in the matrisome due to altered FN splicing.

Because we were interested not only in the matrix proteins, but also the matrix-associated proteins (e.g. apolipoproteins and coagulation factors) which might be regulated in the low-flow response, we took parallel approaches to identify proteins in both the insoluble matrix and proteins in the soluble extracted fractions (Figure 1A&B). At the 7-day endpoint, we perfused the vasculature with cell-impermeable Sulfo-NHS-biotin, and then quenched this activity with glycine. Staining of biotin with streptavidin-594 shows extensive labeling in the artery wall (Figure 1B). Such labeling was not seen in the brain, where signal was confined to the endothelial layer, and is consistent with biotin leak across the endothelium and into the media and adventitia in the low-flow artery. During subsequent processing of the insoluble extracellular matrix by salt and detergent extraction, we retained the soluble supernatants. The biotin-tagged proteins could then be extracted from the pooled soluble fractions by neutravidin bead pull-down, allowing us to examine both the extracted and the insoluble fractions.

Western blots confirmed the desired enrichment of matrix proteins in the final insoluble pellet using this method, as well as extraction/removal of cytoskeletal components and histones (SI Figure 2). Digested samples were assayed by Tandem Mass Spectrometry (TMT) following basic reverse-phase separation. We found ~50% of the peptide spectral intensity coming from defined matrisome proteins in the insoluble fraction (SI Figure 3), and ~25% in the pooled soluble extracted fractions. Although soluble and insoluble samples were run separately, and therefore do not allow a quantitative comparison of signal intensity for specific proteins across samples, spectral intensity analysis supports the expected enrichments of soluble and insoluble proteins in the specific groups. For example, albumin was a greater percentage of signal intensity in the soluble extracted fractions than in the insoluble fraction, while basement membrane collagens (type IV collagens)

were a greater percentage of the insoluble than soluble signal (SI Figure 3). Albumin is only one of many blood proteins we detected, and so we included abundant blood proteins in our analysis, using a list we created from proteins previously found at high abundance in blood [27], and those we detected by analysis of serum (Supplemental Table 1). In the combined soluble and insoluble fractions, 169 matrisome and abundant blood proteins were detected (Figure 1C&D).

To determine how alterations in blood flow modify the representation of matrisome and blood proteins in the insoluble and soluble fractions, we examined changes in matrisome and common blood protein components over their levels in contralateral normal-flow arteries, in both *FnAB-null* and *FnAB-het* mice (6 low-flow and 4 contralateral). Carotids were pooled by genotype and flow response to increase protein content and normalize effects of hemorrhage, as depicted (SI Figure 1). Clustering indicated that flow response, rather than genotype, was the dominant effect in the data (SI Figure 4). Indeed, there was a strong correlation between the low-flow response of *FnAB-null* and *FnAB-het* mice (R^2=0.79) (Figure 2A). Soluble fractions from the same arteries were also correlated (R^2=0.78) (SI Figure 5).

Insoluble FN was ~5 fold (~2.2 Log 2) increased in the low-flow arteries of both *FnAB-null* and *FnAB-het* mice (Figure 2A&C). Four unique peptides specific to the EIIIA segment of FN showed an even greater ~10-fold increase in the low-flow artery over the contralateral control (Figure 2B, Supplemental Table 2). EIIIB-specific peptides were not detected in the MS data. Some of the abundant blood proteins, including Factor II (thrombin), Factor XIIIb (transglutaminase), and a number of Apolipoproteins showed a similar pattern (red dots in Figure 2A, individual proteins shown in bar plots in SI Figure 5 and SI Table 2). This pattern is consistent with increased leak of proteins from blood into the arterial wall of the low-flow carotid artery. However, a few proteins increased more in the low-flow insoluble fraction than in the soluble fraction. Examples include FN, VTN, C3 and APOE (Figure 2C). In contrast, ALB was increased in the soluble fraction and not in the insoluble fraction (Figure 2C). This may suggest selective recruitment or binding to the salt and detergent insoluble fraction in the matrisome response to low flow. Overall, we found 90 matrisome or blood proteins differentially detected in the insoluble or soluble fraction of the low-flow response of either the *FnAB-null* or the *FnAB-het* mice (SI Figure 5 and Supplemental Table 2, $P<0.05$ in at least one comparison with 2 peptides).

Thus, low flow induces reproducible changes in the composition of the vessel wall, including increases in FN and specifically in FN-splice isoform EIIIA. EIIIB containing isoforms were not detected, but this is more likely a limitation in MS detection as EIIIB containing protein isoforms have been observed in these conditions [12]. In general, changes in the soluble and insoluble proteins were similar, with a few exceptions. A large number of the proteins found in increased abundance in both soluble and insoluble fractions are also abundant in the circulation, including FN (Figure 2, SI Figure 5 and SI Table 2).

Absence of FN splice isoforms EIIIA and EIIIB affects flow-induced matrisome composition

Given the prominent changes in FN splice isoform deposition under low and disturbed flow, and our earlier findings that these splice isoforms were important in protecting the arterial wall under low and disturbed flow conditions [12], we asked whether changes in FN splicing altered the matrisome by looking for differences between *FnAB-null* vs *FnAB-het* arteries (Figure 3A&B). There were no detectable differences in total FN protein levels, which were increased in the low-flow arteries in both *FnAB-null* and *FnAB-het* mice (Figure 3C&D). The same was true of most of the matrix differences between low-flow and contralateral arteries. Nevertheless, several interesting differences were detected. Fibrillar collagens (COL1A, COL2A1, COL3A1), which were reduced in low flow arteries of *FnAB-het* mice, were not significantly reduced in the low flow

arteries of *FnAB-null* mice. Dermatopontin (DPT) showed a similar pattern. Conversely, complement C1QB was increased in both *FnAB-null* and *FnAB-het* arteries under low flow, but was increased to a greater degree in the *FnAB-null* mice – its protein partners C1QA and C1QC were not detected. C1QB has previously been shown to bind directly to FN [28]. SERPINB6, also known as Placental thrombin inhibitor, is increased only in *FnAB-het* arteries and not in the *FnAB-null* arteries. Vitronectin (VTN), galectin-1 (LGALS1), and fibulin-1 (FBLN1) showed a similar pattern of increased recruitment in low-flow conditions but only in *FnAB-het* arteries. Differences in the soluble fraction were fewer (Figure 3B).

These matrix changes generally fell into two classes; proteins which were reduced in the matrisome of both *FnAB-null* and *FnAB-het* arteries in low-flow conditions, but less so in *FnAB-null* arteries (e.g. COL1A1, COL2A1, COL3A1, DPT) and proteins which were increased in *FnAB-het* arteries in low-flow conditions, but less so in *FnAB-null* arteries (e.g. SERPINB6B, COL23A1, VTN, LGALS1, FBLN1). Thus, we conclude that without the production of the Fn-EIIIA and -EIIIB inclusive splice isoforms, several of the matrisome changes observed under low flow-conditions failed to occur.

Absence of FN splice isoforms EIIIA and EIIIB affects the binding of serum proteins to activated endothelium *in vitro*

Some of the matrisome changes affected by the splicing of FN are abundant blood proteins (FBLN1, VTN, C1qb, C3), suggesting the possibility that altered FN splicing affects the recruitment of these proteins from the blood. The sub-endothelial matrix is the first layer of matrix which blood proteins encounter when passing into the arterial wall, and FN splice variants are abundant in this matrix [12, 29]. To test directly the hypothesis that changes in FN splice isoforms in matrix produced by endothelial cells affect the binding of proteins from the blood, we prepared conditionally immortalized aortic endothelial cell lines from *FnAB-null* and littermate *FnAB-het* mice and cultured them in the presence of human serum (Figure 4 and SI Figure 6). Since the FN splice isoforms are strongly conserved between mouse and human and expressed by aortic endothelial cells in culture, we reasoned that many important interactions between the mouse FN splice variants and human proteins would also likely be conserved. By combining human serum with mouse aortic endothelial cells, we could distinguish the serum-derived proteins by their unique (human) peptide signatures in mass spectrometry [30]. Furthermore, by biotinylating the human serum prior to addition to mouse cells, we could enrich these proteins by biotin pull-down. Thus, through a combination of biotinylation of serum proteins and MS analysis of human-specific peptide sequences, our methods would enrich and identify serum proteins differentially recruited to a simplified *in vitro* model of the endothelial matrisome, with and without the FN-EIIIA- and EIIIB-containing isoforms.

1%DOC insolubility has been used to assess the incorporation of proteins into extracellular matrix *in vitro* [6, 31], therefore, after extensive PBS washes, we separated the proteins that remained bound to cells and matrix into 1% DOC soluble and insoluble fractions. We found that the biotinylated serum proteins bound to the cellular monolayer were clearly different in their relative intensities from the serum proteins in the culture medium, indicating selective recruitment (SI Figure 6-8). Notably, FN, FBLN1 and serum amyloid (APCS) were strongly enriched among the bound proteins, relative to serum (SI Figure 8C, Supplemental Table 3). Using FN and albumin as examples, FN contributions to the cell/matrix-bound soluble and insoluble fractions increased, as they decreased for albumin (SI Figure 8D). Thus, some proteins are specifically recruited to endothelial cellular monolayers from serum.

471 Having established this system for the analysis of recruited serum proteins, we asked whether
472 there were differences in the recruitment to *FnAB-null* vs. *FnAB-het* endothelial monolayers. In a
473 TMT-labeled quantitative experiment, we defined the relative changes in the recruitment of human
474 proteins to each type of monolayer for the 1% DOC-soluble fraction as well as the 1% DOC-
475 insoluble fraction (Figure 4). An examination of human-specific peptides showed that, of the 90
476 human serum proteins we identified, FBLN1 was strongly impaired in recruitment to the *FnAB-null*
477 monolayer (Figure 4A). We observed a similar result looking at ambiguous peptides, that is
478 additional peptides shared between mouse and human FBLN1 (Figure 4B-C). We believe that the
479 FBLN1 we detect is derived from human serum, and not the cultured mouse endothelial cells. This
480 is consistent with the absence of mouse-specific FBLN1 peptides in our data, and the very low
481 levels of expression of *Fbln1* in mouse endothelial cells *in vitro*, and *in vivo* (<4 FPKM) versus *FN*
482 (500-1000 FPKM) [17].
483
484 Unlike FBLN1, which was strikingly deficient in its recruitment to the DOC-soluble fraction of *FnAB-*
485 *null* endothelial monolayers, the majority of FBLN2 and FBLN5 were found in the 1% DOC
486 insoluble fraction, where they also showed trends towards a reduction in *FnAB-null* vs *FnAB-het*
487 cells. Also unlike FBLN1, these proteins did not show human-specific peptides, consistent with
488 their high levels of expression in arterial endothelium (FPKM ~100-300) [17]. Differences in the
489 levels of the fibulins did not appear to be a result of a general defect in matrix assembly, since we
490 observed similar levels of 1% DOC-insoluble FN (Figure 4D&E), and basement membrane
491 components (COL4A2, LAMA5, LAMC1, LAMB1, SI Figure 9) in the insoluble matrix, regardless of
492 whether cells were *FnAB-null* or *FnAB-het*. In addition to the fibulins, several other proteins also
493 showed impaired recruitment to endothelial monolayers of *FnAB-null* versus *FnAB-het* cells,
494 including BGN, MFGE8, TGFB2 and THBS1 (SI Figure 9 and SI Table 2). For many of these, the
495 impact of altered recruitment to endothelial matrix remains unclear *in vivo*, since they were not
496 detected in the more complex *in vivo* proteome. Some other proteins (e.g. VTN) were detected *in*
497 *vivo* and *in vitro*, but exhibited different responses – increased recruitment to FnAB-null *in vitro*
498 (Figure 4), but reduced *in vivo* (Figure 3). This may be due to differences in the extraction methods
499 or perhaps the specific focus on endothelial interactions *in vitro*. Supporting the latter, quantitative
500 immunofluorescence analysis of VTN in the intima shows a trend towards increased abundance in
501 FnAB-null mice (SI Figure 10), consistent with *in vitro* data.
502
503 Together, our data indicate that FBLN1 is recruited from serum to matrices produced by *FnAB-het*
504 cells, and that this recruitment is impaired in *FnAB-null* cells, replicating the defect in FBLN1
505 recruitment to low-flow arteries in *FnAB-null* mice observed *in vivo*.
506
507 **Splice isoforms of FN are required for the *in vitro* development of FBLN1-based fibrils**
508 To investigate further the differences we had observed by proteomic analysis, we examined the
509 level of FBLN1 in the DOC-soluble fraction of the aortic endothelial cell lines we had examined in
510 proteomic analyses, as well as additional similarly derived aortic endothelial cell lines not included
511 in those analyses. We measured FBLN1 and FN in the DOC-soluble fraction by western blot
512 (Figure 5A), and found that the ratio of FBLN1 to FN was reduced in *FnAB-null* cells, relative to
513 that in *FnAB-het* cells (Figure 5B), concordant with our proteomic results.
514
515 Prior work had shown a nearly complete overlap between FBLN1 and FN fibrils in cultured
516 fibroblasts [32]. However, the relative distributions in endothelial cells, which make very little of
517 their own FBLN1, has not been examined. To our surprise, immunofluorescence of cultured cells at
518 early (Day 3 & Day 7) time points showed that FN fibrils were found along a portion of the FBLN1
519 fibrils, but that there were sections of FBLN1 fibrils without strong FN staining (Figure 5C&D and SI

Figure 11). This resulted in a much higher FBLN1:FN ratio in FnAB-het cells than in FnAB-null cells (Figure 5B), consistent with proteomic and western analyses.

The extensive FBLN1 fibrils despite minimal FN fibrils was surprising. To examine this more closely, we assessed FBLN1 and FN fibrils at high magnification. The deficiency appeared to be due to reductions in FBLN1 fibrils beneath FnAB-null cell bodies, where limited FN fibrils were observed at this timepoint (SI Figure 12). Both FBLN1 and FN deposition could be blocked by forskolin, which inhibits FN fibrillogenesis (SI Figures 11 and 13).

Thus, FBLN1 is deposited in a fibrillar network by *FnAB-het* endothelial cells, this deposition is deficient in *FnAB-null* cells, and FBLN1 deposition is impaired by treatments blocking FN deposition. Interestingly, we note that FBLN1 fibrils are more extensive than the FN fibrils, though they tend to occur in a similar pattern and nearly all FN fibrils are also FBLN1+.

Discussion

Here, we provide evidence that alternative FN splicing, which is induced by platelet and macrophage recruitment under low and disturbed flow [12], affects the matrisome of the arterial wall. Using quantitative mass spectrometry, we quantify changes in the abundance of matrisome proteins induced by low and disturbed flow. We also develop and characterize an *in vitro* model for the recruitment of blood proteins into the endothelial matrisome. Increased amounts of FN splice variants are found in the arterial wall under low flow, and genetic suppression of the alternative splicing of FN affects the recruitment of FBLN1 and other blood-derived proteins, revealing a novel mechanism through which FN splicing could impact vascular development and disease.

Changes in matrisome composition of the vascular wall in the early response to low flow

Reduced flow induces widespread changes in the matrisome as early as 7 days after alterations in blood flow. A key advantage of this model is that by controlling the initiation of low-flow conditions, the very earliest stages of low-flow-mediated matrisome changes can be observed. In this early stage, in addition to the increases in FN deposition which have been well described [7, 8, 33, 34], we observe both increases and decreases in a large number of other matrisome proteins. Other increased proteins include collagen VIII, a regulator of smooth muscle cell proliferation and growth [35], collagen XI, a key contributor to collagen fibrillogenesis [36], and FBLN1 and FBLN2, regulators of basement membrane formation with overlapping and compensatory expression in arterial remodeling [37]. A few notable examples of decreased proteins include latent transforming growth factor beta binding protein 4 (LTBP4), an important regulator of TGFβ signaling [38], the microfibril-associated proteins MFAP2 and MFAP4, also important in regulation of TGFβ signaling and Notch signaling [39], and the basement membrane components laminins and collagen IV. Many of these proteins are similarly regulated in chronic models of atherosclerosis in mouse [40], and in samples from symptomatic vs. non-symptomatic human plaque [41]. While the functions of some of these proteins have already been validated in atherogenesis in mouse models, the functions of most remain unknown.

Effect of FN splice variants on FBLN1 recruitment

Our data show that recruitment of FBLN1 to the artery wall *in vivo*, and to an endothelial monolayer *in vitro* is dependent on FN splice variants including alternative exons EIIIA and EIIIB. FN is the dominant matrix protein responsible for binding and recruitment of FBLN1 to the matrix [42]. Those prior studies showed no difference in the binding of FBLN1 to “cellular” FN, which generally contains EIIIA and EIIIB, or plasma FN, which generally does not [42]. However, it is likely that the way in which those studies were conducted obscured changes in FN conformation within a cell-

derived matrix. In those experiments, FN was bound to plastic, a process which is known to expose cryptic sites within the FN molecule [6]. Indeed, in those studies, the authors had noted that they were unable to use soluble FN to interfere with the binding of FBLN1 in solution to FN immobilized on plastic [42]. This suggests that FBLN1 binds domains in the immobilized FN not exposed in soluble protein. Although our data could also be consistent with FBLN1 binding to FN through an intermediate, we think a plausible hypothesis is that the inclusion of EIIIA promotes the exposure of cryptic binding sites in FN. Notably, FN binding to FBLN1 occurs through an interaction with FN type III repeats 13-14, which are adjacent to the EIIIA domain between the 11th and 12th type III repeats. There is precedent for this, as inclusion of EIIIB exposes a cryptic antibody binding site in the adjacent 7th type III domain [43], and EIIIA itself is also cryptic until exposed by proteolytic cleavage [44]. Thus, we suggest that the FBLN1 binding site is present in all FN molecules, but that the inclusion of EIIIA and EIIIB promotes exposure of this cryptic binding site in cell-derived matrices.

FBLN1 (*Fbln1*) plays an important role in vascular development [45]. Recruitment of FBLN1 is likely to be important for biological functions, as endothelial cells produce very little *Fbln1* transcript themselves *in vivo* or *in vitro* (FPKM ~2-4 versus *Fbln2* and *Fbln5*, which are FPKM ~100-300), under both normal or low and disturbed flow conditions [17, 46]. Both plasma and adjacent mural cells could contribute to the FBLN1 in the basement membrane [46], but there may be developmental or disease settings where the main source of FBLN1 is the plasma. In these instances, the splicing of FN may provide an important signal for FBLN1 recruitment. Thus, we might expect to see similar phenotypes in *Fbln1*-deficient and splicing-deficient mice. Indeed, during embryonic development, where FN EIIIA and EIIIB inclusion is particularly high, both *Fbln1-null* and *FnAB-null* embryos display a partially penetrant embryonic lethality with major microvascular defects and hemorrhage [45, 47]. In response to lung injury, FN EIIIA and EIIIB inclusion is also increased. In this response, both *FnA-null* mice and *Fbln1c-null* mice exhibit reduced lung fibrosis [48, 49]. As FBLN1 has been linked to premature atherosclerosis [11], aortic dissection [50, 51] and arterial stiffness [52], the effect of FN splicing on FBLN1 recruitment to the arterial intima may be important in these processes as well. Furthermore, as mutations in other basement membrane proteins promote vessel hemorrhage [53] and are linked to coronary artery disease, atherosclerosis and artery stiffening [54], and impaired FN splicing has been observed in cells isolated from a patient population with increased risk of aortic aneurysm and dissection [55], increased understanding of trans- and cis-regulatory mechanisms of FN splicing could reveal novel genetic mediators in human vascular disease.

Effect of FN splice variants on recruitment of other proteins

Although we have observed prominent effects of alternative FN splicing on the recruitment of FBLN1 from the serum to endothelial cell monolayers, there are a number of other serum-derived proteins that are similarly affected (Figure 3 and 4 and SI Figure 5 and SI Table 2). However, many of the proteins affected *in vitro* were either not detected *in vivo*, or detected but not significantly altered *in vivo*. This is perhaps not surprising given the differences in the experimental approaches to assess the proteome of the arterial wall *in vivo*, and the matrix from cultured cells *in vitro*. Notable differences between the *in vivo* and *in vitro* models include the contributions of multiple cell types to the matrix *in vivo* (e.g. smooth muscle cells, immune cells, fibroblasts), culture in clotted blood (serum) versus circulating plasma, and the presence of physical factors (e.g. disturbed blood flow, and intraluminal pressure) which may drive blood proteins across the vessel wall along a pressure gradient. Nevertheless, the *in vitro* system suggested effects of FN splicing on the recruitment of a number of proteins relevant to the response of the arterial wall, including Lactadherin (MFGE8), which promotes apoptotic cell uptake via Integrin $\alpha V\beta 3$ [56], Biglycan (BGN) which is a binding partner of ldl [57], and Thrombospondin-1 (THBS1) and Transforming

519 Growth Factor Beta (TGFB2), which have critical functions in coagulation, extracellular matrix
520 production and immune cell signaling [58]. Future directed analysis of the proteins defined *in vitro*
521 may reveal focal defects in their recruitment within the artery wall, e.g. altered localization to the
522 arterial intima adjacent the endothelium vs. medial or adventitial layers.
523
524 In conclusion, we have demonstrated that altered splicing of FN can change matrix composition by
525 acutely affecting the recruitment of circulating proteins with potentially critical functions in vascular
526 development and disease, revealing new ways in which alternative splicing of FN may exert
527 functional effects.
528

Acknowledgments:
We thank members of the Hynes lab and other labs in the Koch Institute for advice and discussions, particularly Alexandra Naba for discussions of matrisome and matrisome enrichment. We thank the Swanson Biotechnology Center at the Koch Institute/MIT, especially the Applied Therapeutics & Whole Animal Imaging Facility, the Hope Babette Tang (1983) Histology Facility, the Microscopy Facility, the Barbara K. Ostrom (1978) Bioinformatics and Computing Facility, the Koch Institute Flow Cytometry Core and Scott Malstrom and Charlie Whittaker for their expert support. We also thank Stuart Levine and Vincent Butty in the MIT BioMicro Center, for help with RNA analysis. The authors wish to dedicate this paper to the memory of Officer Sean Collier for his caring service to the MIT community.

Sources of Funding:
This work was supported by UCONN Health startup funds and NIH NHLBI grant to PAM (K99/R00-HL125727) and by the Howard Hughes Medical Institute of which ROH was an Investigator. NJ was funded by a Mazumdar-Shaw International Oncology Fellowship. The Swanson Biotechnology Centers at the Koch Institute/MIT were supported in part by the Koch Institute Support (core) Grant P30-CA14051 from the National Cancer Institute and by Koch Institute funds.

References:

1. Tabas, I., G. Garcia-Cardena, and G.K. Owens, *Recent insights into the cellular biology of atherosclerosis.* J Cell Biol, 2015. **209**(1): p. 13-22.
2. Baeyens, N., et al., *Endothelial fluid shear stress sensing in vascular health and disease.* J Clin Invest, 2016. **126**(3): p. 821-8.
3. Gimbrone, M.A., Jr. and G. Garcia-Cardena, *Endothelial Cell Dysfunction and the Pathobiology of Atherosclerosis.* Circ Res, 2016. **118**(4): p. 620-36.
4. Stone, P.H., et al., *Prediction of progression of coronary artery disease and clinical outcomes using vascular profiling of endothelial shear stress and arterial plaque characteristics: the PREDICTION Study.* Circulation, 2012. **126**(2): p. 172-81.
5. Ross, R., *Atherosclerosis--an inflammatory disease.* N Engl J Med, 1999. **340**(2): p. 115-26.
6. Singh, P., C. Carraher, and J.E. Schwarzbauer, *Assembly of fibronectin extracellular matrix.* Annu Rev Cell Dev Biol, 2010. **26**: p. 397-419.
7. Orr, A.W., et al., *The subendothelial extracellular matrix modulates NF-kappaB activation by flow: a potential role in atherosclerosis.* J Cell Biol, 2005. **169**(1): p. 191-202.
8. Rohwedder, I., et al., *Plasma fibronectin deficiency impedes atherosclerosis progression and fibrous cap formation.* EMBO Mol Med, 2012. **4**(7): p. 564-76.
9. Huang, L.H., et al., *Interleukin-17 Drives Interstitial Entrapment of Tissue Lipoproteins in Experimental Psoriasis.* Cell Metab, 2019. **29**(2): p. 475-487 e7.
10. Argraves, W.S., et al., *Fibulin-1 and fibrinogen in human atherosclerotic lesions.* Histochem Cell Biol, 2009. **132**(5): p. 559-65.
11. Bhosale, S.D., et al., *Serum Proteomic Profiling to Identify Biomarkers of Premature Carotid Atherosclerosis.* Sci Rep, 2018. **8**(1): p. 9209.
12. Murphy, P.A. and R.O. Hynes, *Alternative splicing of endothelial fibronectin is induced by disturbed hemodynamics and protects against hemorrhage of the vessel wall.* Arterioscler Thromb Vasc Biol, 2014. **34**(9): p. 2042-50.
13. Astrof, S. and R.O. Hynes, *Fibronectins in vascular morphogenesis.* Angiogenesis, 2009. **12**(2): p. 165-75.
14. Vizcaino, J.A., et al., *2016 update of the PRIDE database and its related tools.* Nucleic Acids Res, 2016. **44**(22): p. 11033.
15. Ni, C.W., et al., *Discovery of novel mechanosensitive genes in vivo using mouse carotid artery endothelium exposed to disturbed flow.* Blood, 2010. **116**(15): p. e66-73.
16. Kobayashi, M., et al., *A simple method of isolating mouse aortic endothelial cells.* J Atheroscler Thromb, 2005. **12**(3): p. 138-42.
17. Murphy, P.A., et al., *Alternative RNA splicing in the endothelium mediated in part by Rbfox2 regulates the arterial response to low flow.* Elife, 2018. **7**.
18. Zhao, J.J., et al., *Human mammary epithelial cell transformation through the activation of phosphatidylinositol 3-kinase.* Cancer Cell, 2003. **3**(5): p. 483-95.
19. Naba, A., K.R. Clauser, and R.O. Hynes, *Enrichment of Extracellular Matrix Proteins from Tissues and Digestion into Peptides for Mass Spectrometry Analysis.* J Vis Exp, 2015(101): p. e53057.
20. Cox, J. and M. Mann, *MaxQuant enables high peptide identification rates, individualized p.p.b.-range mass accuracies and proteome-wide protein quantification.* Nat Biotechnol, 2008. **26**(12): p. 1367-72.
21. Huang, F.K., et al., *Deep Coverage of Global Protein Expression and Phosphorylation in Breast Tumor Cell Lines Using TMT 10-plex Isobaric Labeling.* J Proteome Res, 2017. **16**(3): p. 1121-1132.

595 22. Naba, A., et al., *The matrisome: in silico definition and in vivo characterization by proteomics of*
596 *normal and tumor extracellular matrices.* Mol Cell Proteomics, 2012. **11**(4): p. M111 014647.
597 23. Kammers, K., et al., *Detecting Significant Changes in Protein Abundance.* EuPA Open Proteom, 2015.
598 **7**: p. 11-19.
599 24. Efstathiou, G., et al., *ProteoSign: an end-user online differential proteomics statistical analysis*
600 *platform.* Nucleic Acids Res, 2017. **45**(W1): p. W300-W306.
601 25. D'Angelo, G., et al., *Statistical Models for the Analysis of Isobaric Tags Multiplexed Quantitative*
602 *Proteomics.* J Proteome Res, 2017. **16**(9): p. 3124-3136.
603 26. Korshunov, V.A. and B.C. Berk, *Flow-induced vascular remodeling in the mouse: a model for carotid*
604 *intima-media thickening.* Arterioscler Thromb Vasc Biol, 2003. **23**(12): p. 2185-91.
605 27. Hortin, G.L., D. Sviridov, and N.L. Anderson, *High-abundance polypeptides of the human plasma*
606 *proteome comprising the top 4 logs of polypeptide abundance.* Clin Chem, 2008. **54**(10): p. 1608-16.
607 28. Bing, D.H., et al., *Fibronectin binds to the C1q component of complement.* Proc Natl Acad Sci U S A,
608 1982. **79**(13): p. 4198-201.
609 29. Tan, M.H., et al., *Deletion of the alternatively spliced fibronectin EIIIA domain in mice reduces*
610 *atherosclerosis.* Blood, 2004. **104**(1): p. 11-8.
611 30. Naba, A., et al., *Extracellular matrix signatures of human mammary carcinoma identify novel*
612 *metastasis promoters.* Elife, 2014. **3**: p. e01308.
613 31. Choi, M.G. and R.O. Hynes, *Biosynthesis and processing of fibronectin in NIL.8 hamster cells.* J Biol
614 Chem, 1979. **254**(23): p. 12050-5.
615 32. Argraves, W.S., et al., *Fibulin is an extracellular matrix and plasma glycoprotein with repeated*
616 *domain structure.* J Cell Biol, 1990. **111**(6 Pt 2): p. 3155-64.
617 33. Al-Yafeai, Z., et al., *Endothelial FN (Fibronectin) Deposition by alpha5beta1 Integrins Drives*
618 *Atherogenic Inflammation.* Arterioscler Thromb Vasc Biol, 2018. **38**(11): p. 2601-2614.
619 34. Yurdagul, A., Jr., et al., *The arterial microenvironment: the where and why of atherosclerosis.*
620 Biochem J, 2016. **473**(10): p. 1281-95.
621 35. Adiguzel, E., et al., *Migration and growth are attenuated in vascular smooth muscle cells with type*
622 *VIII collagen-null alleles.* Arterioscler Thromb Vasc Biol, 2006. **26**(1): p. 56-61.
623 36. Tompson, S.W., et al., *Fibrochondrogenesis results from mutations in the COL11A1 type XI collagen*
624 *gene.* Am J Hum Genet, 2010. **87**(5): p. 708-12.
625 37. Sicot, F.X., et al., *Fibulin-2 is dispensable for mouse development and elastic fiber formation.* Mol
626 Cell Biol, 2008. **28**(3): p. 1061-7.
627 38. Robertson, I.B., et al., *Latent TGF-beta-binding proteins.* Matrix Biol, 2015. **47**: p. 44-53.
628 39. Mecham, R.P. and M.A. Gibson, *The microfibril-associated glycoproteins (MAGPs) and the*
629 *microfibrillar niche.* Matrix Biol, 2015. **47**: p. 13-33.
630 40. Wierer, M., et al., *Compartment-resolved Proteomic Analysis of Mouse Aorta during Atherosclerotic*
631 *Plaque Formation Reveals Osteoclast-specific Protein Expression.* Mol Cell Proteomics, 2018. **17**(2):
632 p. 321-334.
633 41. Langley, S.R., et al., *Extracellular matrix proteomics identifies molecular signature of symptomatic*
634 *carotid plaques.* J Clin Invest, 2017. **127**(4): p. 1546-1560.
635 42. Balbona, K., et al., *Fibulin binds to itself and to the carboxyl-terminal heparin-binding region of*
636 *fibronectin.* J Biol Chem, 1992. **267**(28): p. 20120-5.
637 43. Balza, E., et al., *A novel human fibronectin cryptic sequence unmasked by the insertion of the*
638 *angiogenesis-associated extra type III domain B.* Int J Cancer, 2009. **125**(4): p. 751-8.
639 44. Julier, Z., et al., *The TLR4 agonist fibronectin extra domain A is cryptic, exposed by elastase-2; use in*
640 *a fibrin matrix cancer vaccine.* Sci Rep, 2015. **5**: p. 8569.

741 45. Kostka, G., et al., *Perinatal lethality and endothelial cell abnormalities in several vessel*
742 *compartments of fibulin-1-deficient mice.* Mol Cell Biol, 2001. **21**(20): p. 7025-34.
743 46. Vanlandewijck, M., et al., *A molecular atlas of cell types and zonation in the brain vasculature.*
744 Nature, 2018. **554**(7693): p. 475-480.
745 47. Astrof, S., D. Crowley, and R.O. Hynes, *Multiple cardiovascular defects caused by the absence of*
746 *alternatively spliced segments of fibronectin.* Dev Biol, 2007. **311**(1): p. 11-24.
747 48. Muro, A.F., et al., *An essential role for fibronectin extra type III domain A in pulmonary fibrosis.* Am J
748 Respir Crit Care Med, 2008. **177**(6): p. 638-45.
749 49. Liu, G., et al., *Fibulin-1 regulates the pathogenesis of tissue remodeling in respiratory diseases.* JCI
750 Insight, 2016. **1**(9).
751 50. Mohamed, S.A., et al., *Pathway analysis of differentially expressed genes in patients with acute*
752 *aortic dissection.* Biomark Insights, 2009. **4**: p. 81-90.
753 51. Cheuk, B.L. and S.W. Cheng, *Differential expression of elastin assembly genes in patients with*
754 *Stanford Type A aortic dissection using microarray analysis.* J Vasc Surg, 2011. **53**(4): p. 1071-1078
755 e2.
756 52. Yasmin, et al., *The matrix proteins aggrecan and fibulin-1 play a key role in determining aortic*
757 *stiffness.* Sci Rep, 2018. **8**(1): p. 8550.
758 53. Gould, D.B., et al., *Mutations in Col4a1 cause perinatal cerebral hemorrhage and porencephaly.*
759 Science, 2005. **308**(5725): p. 1167-71.
760 54. Steffensen, L.B. and L.M. Rasmussen, *A role for collagen type IV in cardiovascular disease?* Am J
761 Physiol Heart Circ Physiol, 2018. **315**(3): p. H610-H625.
762 55. Paloschi, V., et al., *Impaired splicing of fibronectin is associated with thoracic aortic aneurysm*
763 *formation in patients with bicuspid aortic valve.* Arterioscler Thromb Vasc Biol. **31**(3): p. 691-7.
764 56. Hanayama, R., et al., *Identification of a factor that links apoptotic cells to phagocytes.* Nature, 2002.
765 **417**(6885): p. 182-7.
766 57. Neufeld, E.B., et al., *Decorin and biglycan retain LDL in disease-prone valvular and aortic*
767 *subendothelial intimal matrix.* Atherosclerosis, 2014. **233**(1): p. 113-21.
768 58. Adams, J.C. and J. Lawler, *The thrombospondins.* Cold Spring Harb Perspect Biol, 2011. **3**(10): p.
769 a009712.
770

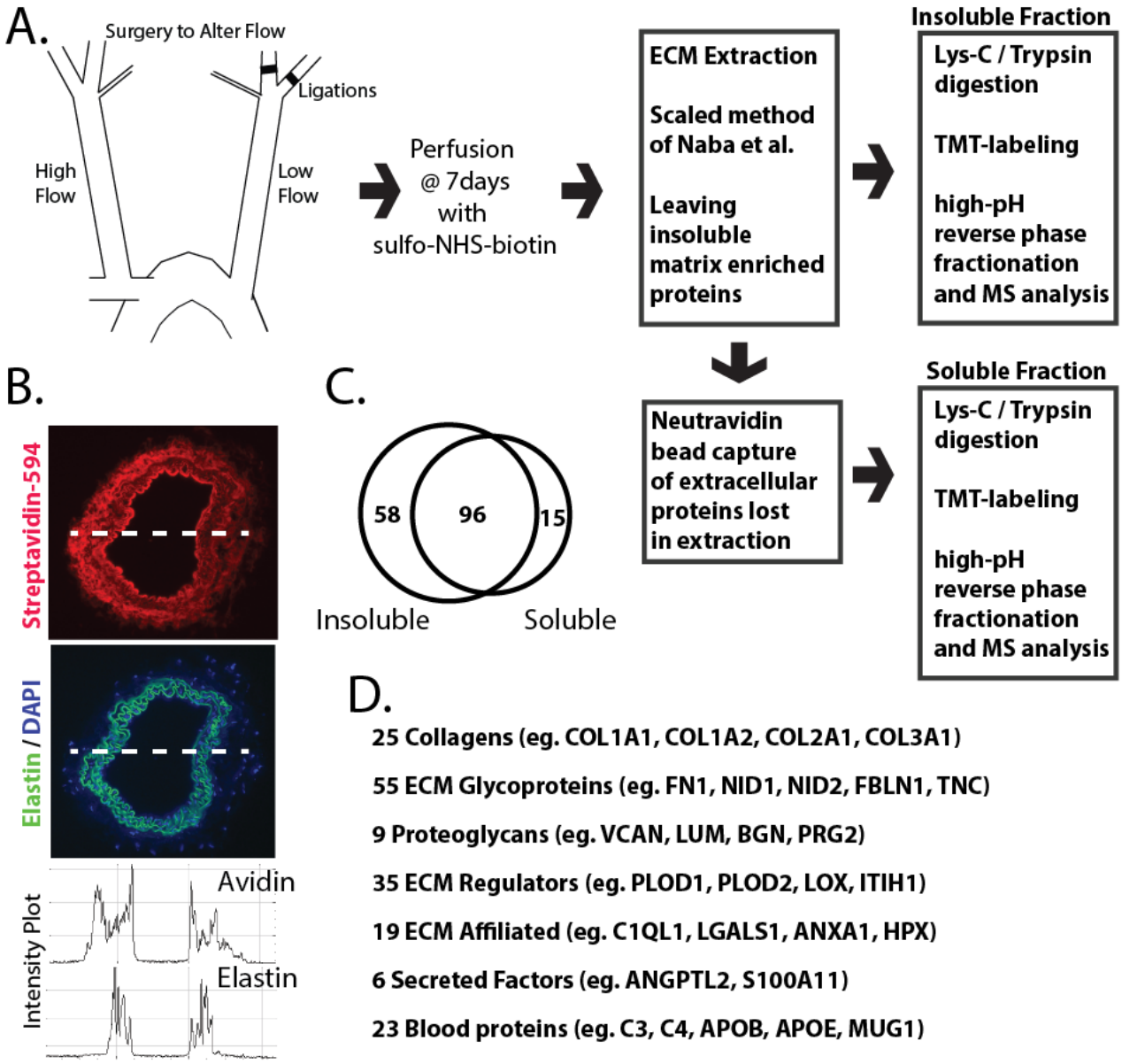

Figure 1. Analysis of matrisome changes in arteries exposed to low and disturbed flow
(A) Schematic of methods for the enrichment of arterial matrisome proteins under varying flow profiles. Partial ligation of the left carotid artery is achieved by complete ligation of the external and internal branches, leaving the thyroid branch patent. Following extracellular biotinylation, pools of vessels from *FnAB-null* and *FNAB-het* mice were harvested and matrisome proteins extracted by defined insolubility in salt and detergent buffers and then digested for mass spectrometry. (B) Streptavidin staining showing labeling of carotid proteins with biotin, and elastin autofluorescence and DAPI of the same section. Intensity plot shows the relative intensity of the streptavidin and elastin signal along the line across the vessel; note the strong avidin signal over the intima. (C) Venn diagram showing total numbers of matrisome and blood proteins isolated in the soluble-extracted and insoluble fractions, and their overlap. (D) Numbers of matrisome and blood proteins found in each category by mass spectrometry, with examples of identified proteins.

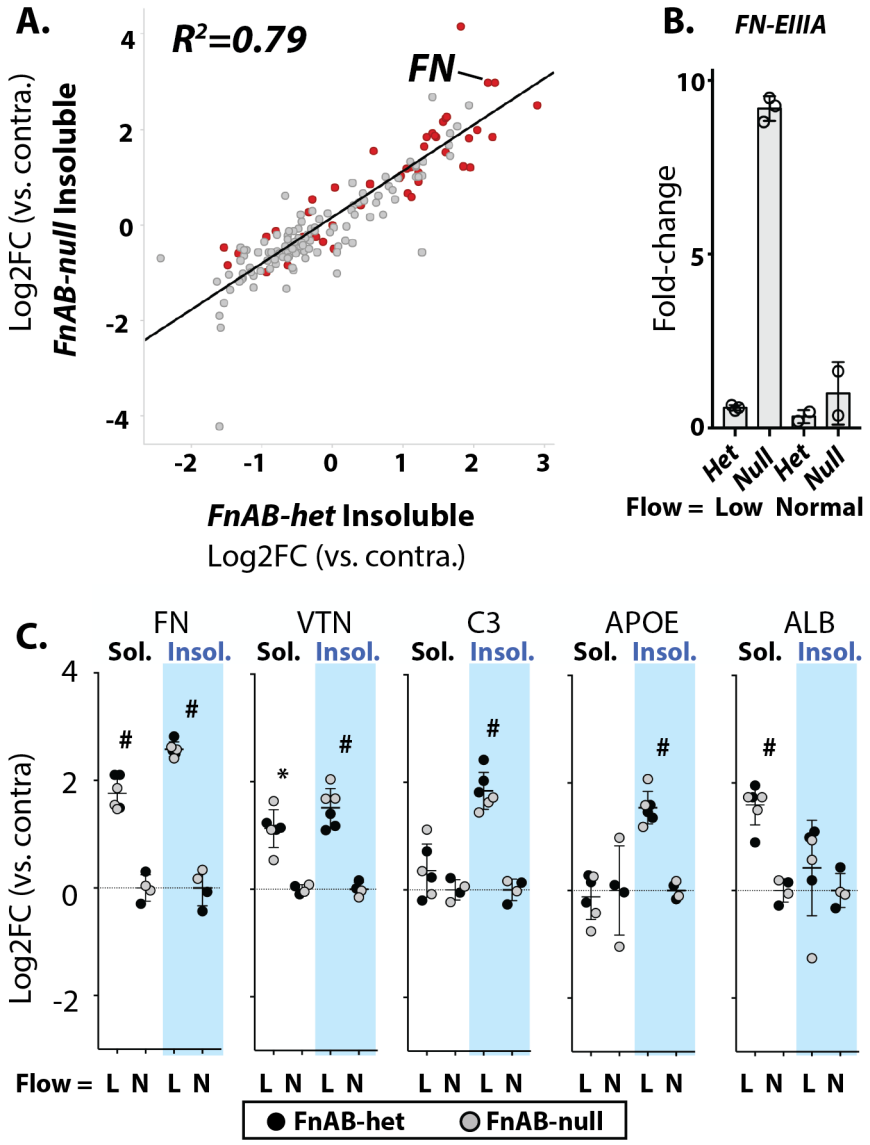

Figure 2. Dynamic regulation of matrisome composition under low and disturbed flow

(A) Plot showing the correlation between the regulation of matrisome and blood-derived protein levels under low flow between *FnAB-het* and *FnAB-null* mice in the insoluble fraction. X and Y axis are Log2 fold-change (low-flow artery vs contralateral normal-flow artery). All points shown represent a single protein with at least two peptides, and points in red mark proteins that are abundant in blood. (B) Abundance of Fn-EIIIA-specific peptides (average of 4 unique) in the various conditions relative to control contralateral arteries under high flow. (C) Graph showing Log2 fold-change under low-flow (L) conditions vs. normal flow contralateral controls (N) for the indicated pools of arteries (grey dots are *FnAB-het* N=3 pools vs N=2 pools and black dots are *FnAB-null* N=3 pools vs N=2 pools), including both soluble (Sol) and insoluble (Insol) fractions. Data for soluble and insoluble fractions were collected from the same arteries as labeled and run in separate mass-spectrometry experiments. They are shown together here for ease of comparisons. Statistical analysis of differences by Limma, as described in the methods (*=P<0.05; #=P<0.005).

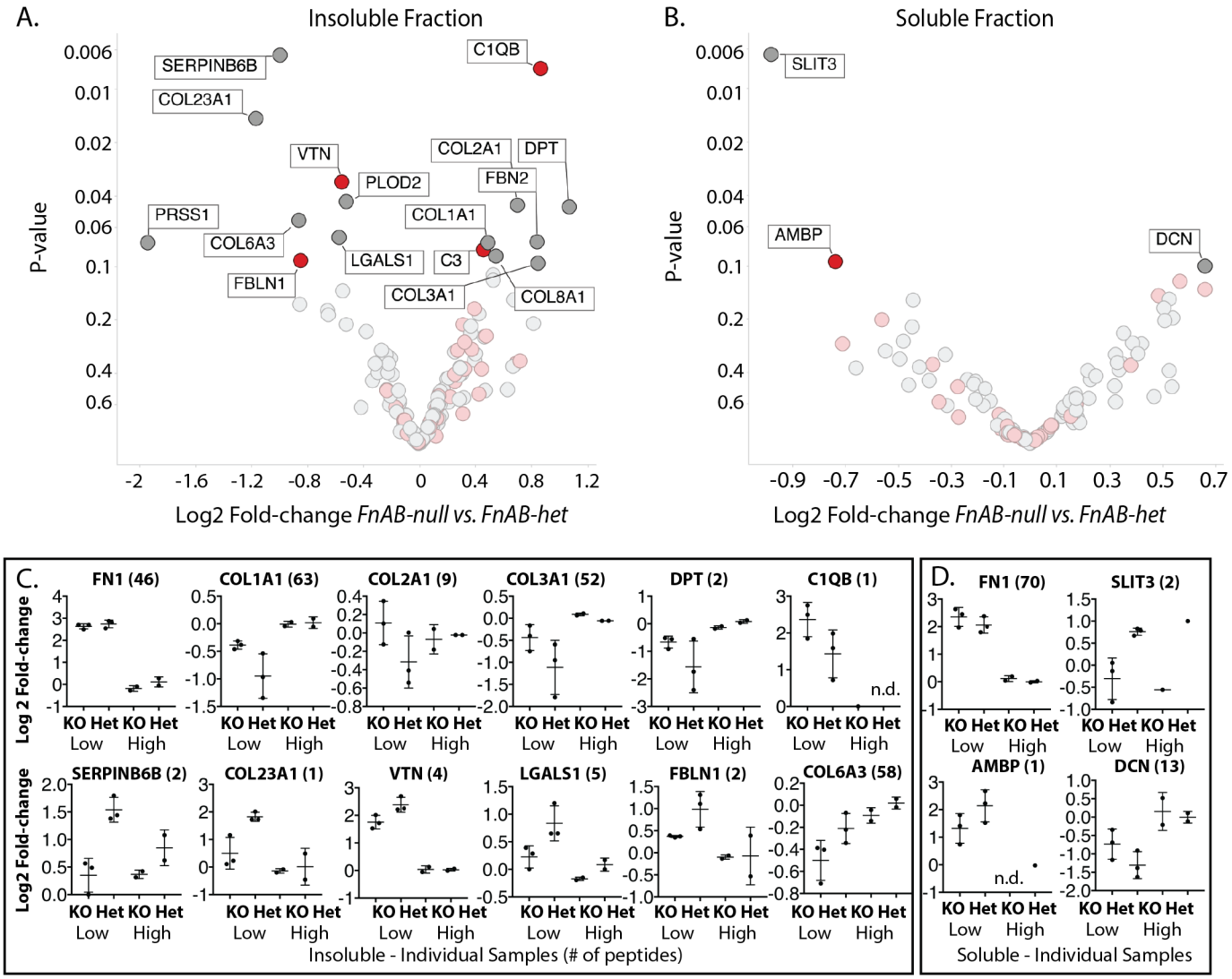

Figure 3. Absence of FN-EIIIA and –EIIIB alters the response of the arterial matrisome to low flow
(A-B) Volcano plots showing the differences in matrisome composition between *FnAB-null* and *FnAB-het* arteries in the (A) insoluble and (B) soluble fraction, as determined by mass spectrometry. Red dots mark proteins that are abundant in blood. Light grey and pink dots are below the unadjusted p-value of 0.1. (C-D) Examples of differences observed in the (C) insoluble and soluble (D) fraction. In C & D, each point is quantitation from a separate pool of arteries by mass spectrometry, based on the number of unique peptides shown in brackets.

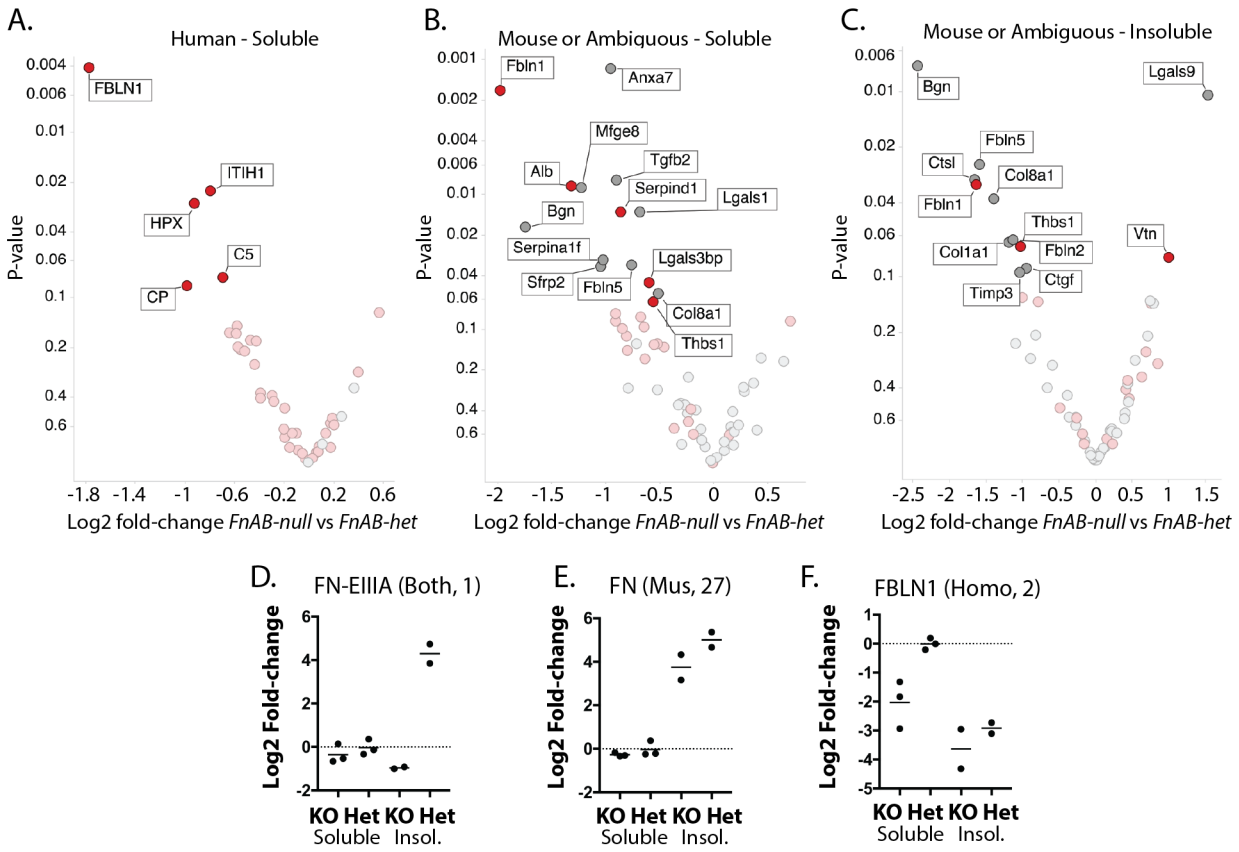

Figure 4. Serum- and cell-derived contributions to the endothelial matrisome *in vitro*
(A-C) Volcano plots showing proteins differentially bound between *FnAB-null* and *FnAB-het* aortic endothelial cells. (A) Human serum-derived proteins in the DOC-soluble fraction (A) and mouse or ambiguous proteins in the DOC-soluble (B) and DOC-insoluble (C) fractions. Red data points mark proteins abundant in blood. Light grey/red data points mark proteins with adj P-value <0.1. (D-E Graphs showing individual differentially regulated proteins. Fold-change is relative to EIIIAB Het, soluble. Each point is a biological replicate. Mus=mouse specific peptide identification, Homo=human specific peptide identification, Both=ambiguous, human or mouse.

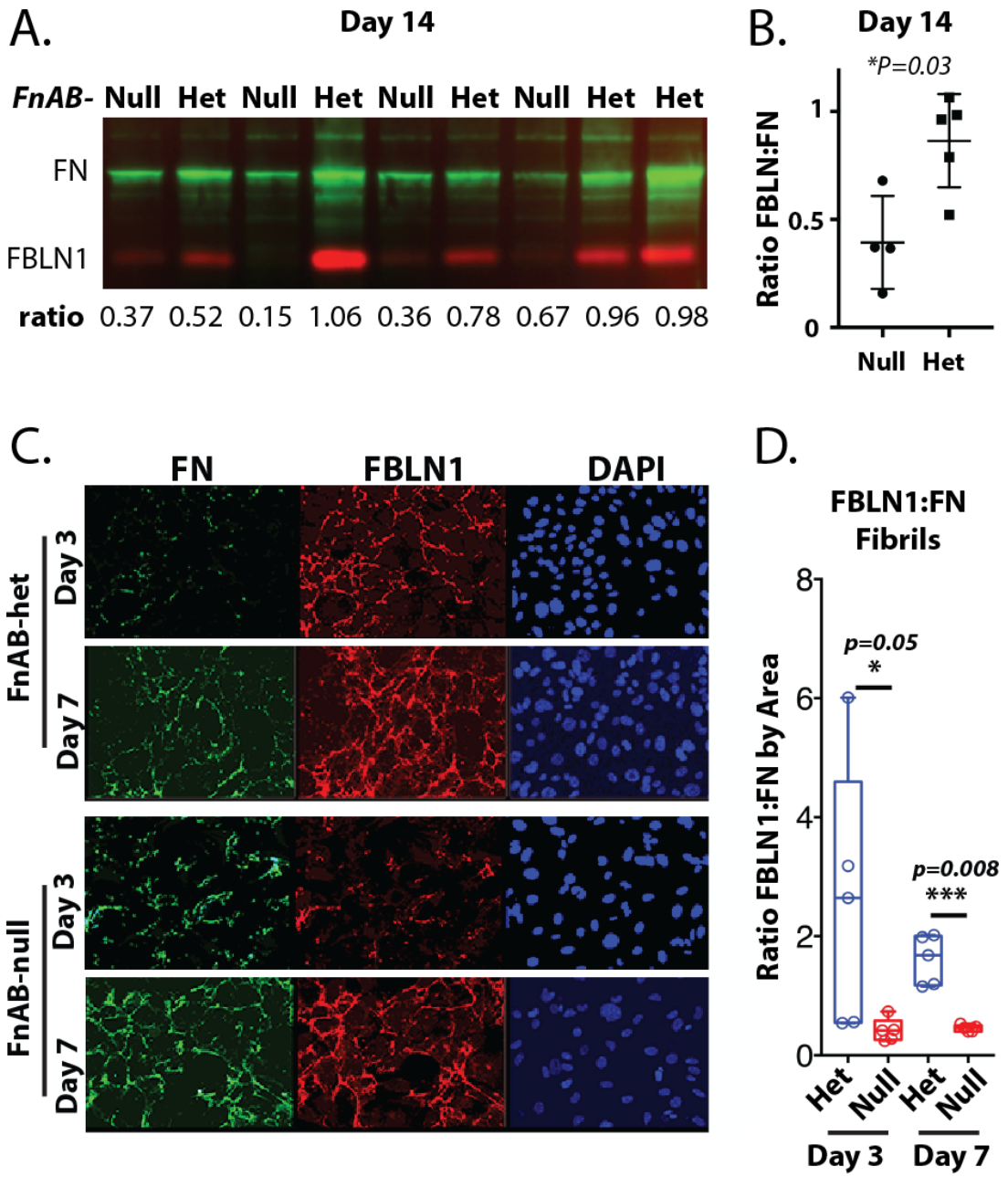

Figure 5. FBLN1 recruitment is dependent on Fibronectin fibrillogenesis and FN EIIIA and EIIIB
(A) Western blot and (B) quantitation showing the levels of Fibulin-1 relative to Fibronectin in the 1% DOC-soluble fraction of aortic endothelial cell lines (N=4 *FnAB-null* and N=5 *FnAB-het*) cultured in human serum. P value is from Mann-Whitney test. (C) Immunofluorescence showing staining for FN and FBLN1 in a pair of *FnAB-het* and *FnAB-null* aortic endothelial cell monolayers in culture with human serum. (D) Quantitation of the relative area covered by FBLN1 and FN fibrils in Day 3 and Day 7 cultures. Statistical analysis is by Mann-Whitney test at each timepoint.

A. Summary of Samples Used in Proteomic Analysis

Genotype	Sex	Hemorrhage (=1)	Severity	Group (Sol)	Group (Insol)
FnAB-Null	M	0	2	1	13
FnAB-Null	M	1	3	1	13
FnAB-Null	M	1	4	1	13
FnAB-Null	M	0	1	2	14
FnAB-Null	F	1	3	2	14
FnAB-Null	M	1	4	2	14
FnAB-Null	F	1	3	3	15
FnAB-Null	F	0	4	3	15
FnAB-Null	F	0	1.5	3	15
FnAB-Het	M	1	3	4	16
FnAB-Het	M	0	3	4	16
FnAB-Het	M	0	4	4	16
FnAB-Het	M	1	4	5	17
FnAB-Het	M	1	4	5	17
FnAB-Het	M	1	4	5	17
FnAB-Het	M	1	3	5	17
FnAB-Het	F	0	3	6	18
FnAB-Het	F	0	1	6	18
FnAB-Het	F	0	1.5	6	18

B. Hemorrhage Frequency

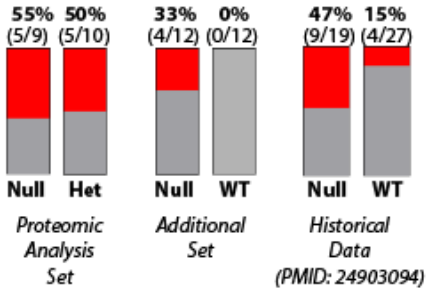

SI Figure 1. Pooling of samples used in proteomics analysis and hemorrhage analysis
(A) Table showing the characteristics of the samples used. Each line indicates an individual mouse. Hemorrhage and severity (degree of fibrotic response) were assessed as described in Murphy & Hynes, ATVB 2014. Group indicates the pool to which the artery was added. Each set of arteries contributed to both a soluble and insoluble pool of protein isolate. For clarity, only the low flow (ligated) pools are shown, but a corresponding contralateral pool existed for each of these. (B) Freqency of visible hemorrhage in the mice used for proteomic analysis (also shown in A), a second set of mice not used for this proteomic data, and historical data from Murphy & Hynes, ATVB 2014.

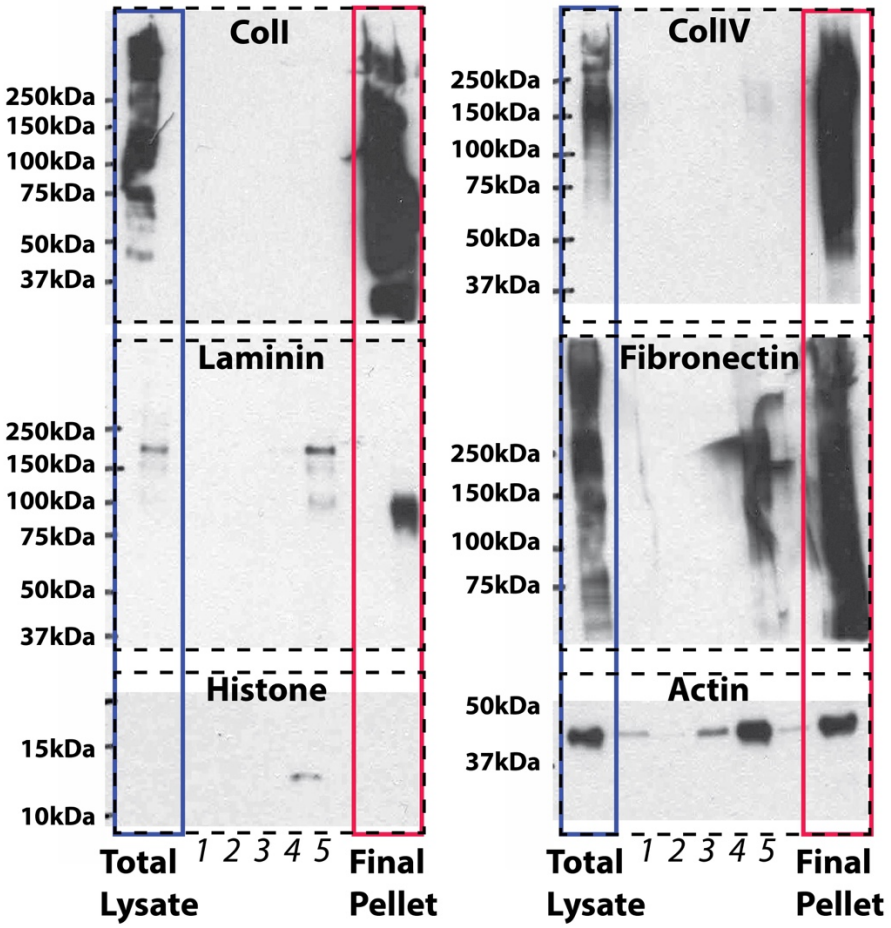

SI Figure 2. Enrichment of detergent insoluble proteins from carotid arteries
Western blots showing fractionation of a 10mg pool of ten wild-type carotid arteries by Compartment Extraction based ECM enrichment protocol (Naba et al. 2012). Sequential steps (1-5) remove cytosolic (1) nuclear (2) membrane (3) cytoskeletal proteins (4), before a final wash (5), leaving the ECM enriched pellet. 20% of each of the wash steps, and all of the final pellet were loaded. Note that some fibronectin and laminin is extracted in steps 4 and 5. The extracted fibronectin likely represents plasma fibronectin from the blood vessels not yet assembled into the matrix. Some portion of the laminin pool may be similarly incompletely incorporated into the insoluble matrix.

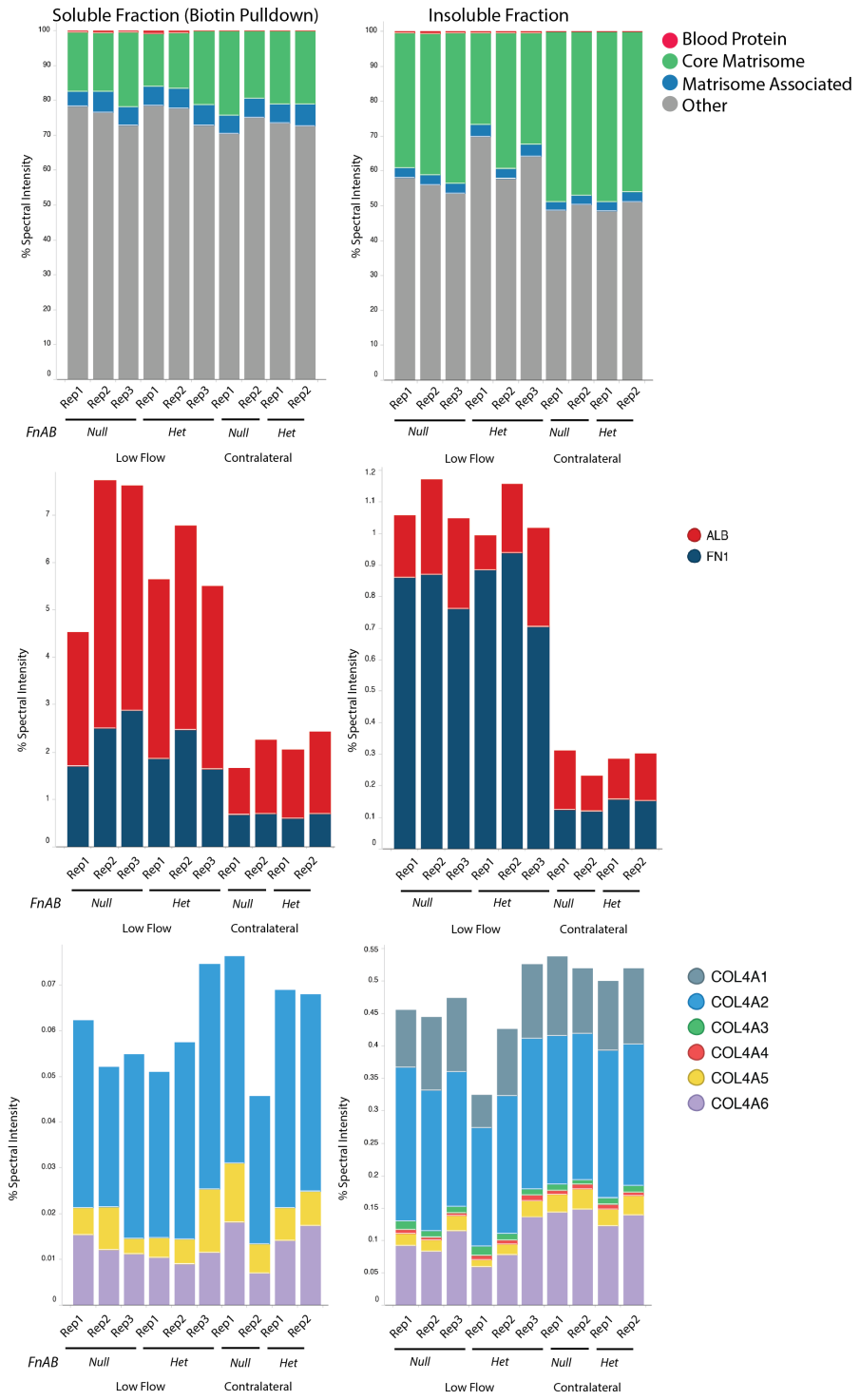

SI Figure 3. Matrisome proteins as a percent of summed spectral intensities from mass spectrometry
Figures show the spectral intensities for the indicated pools, as a percentage of all spectral intensities from annotated peptides. "Other" indicates that the protein is not included in the indicated groups, These "Other" proteins are a large set of proteins, each with a relatively low level of spectral intensity, and are not included in our subsequent analysis.

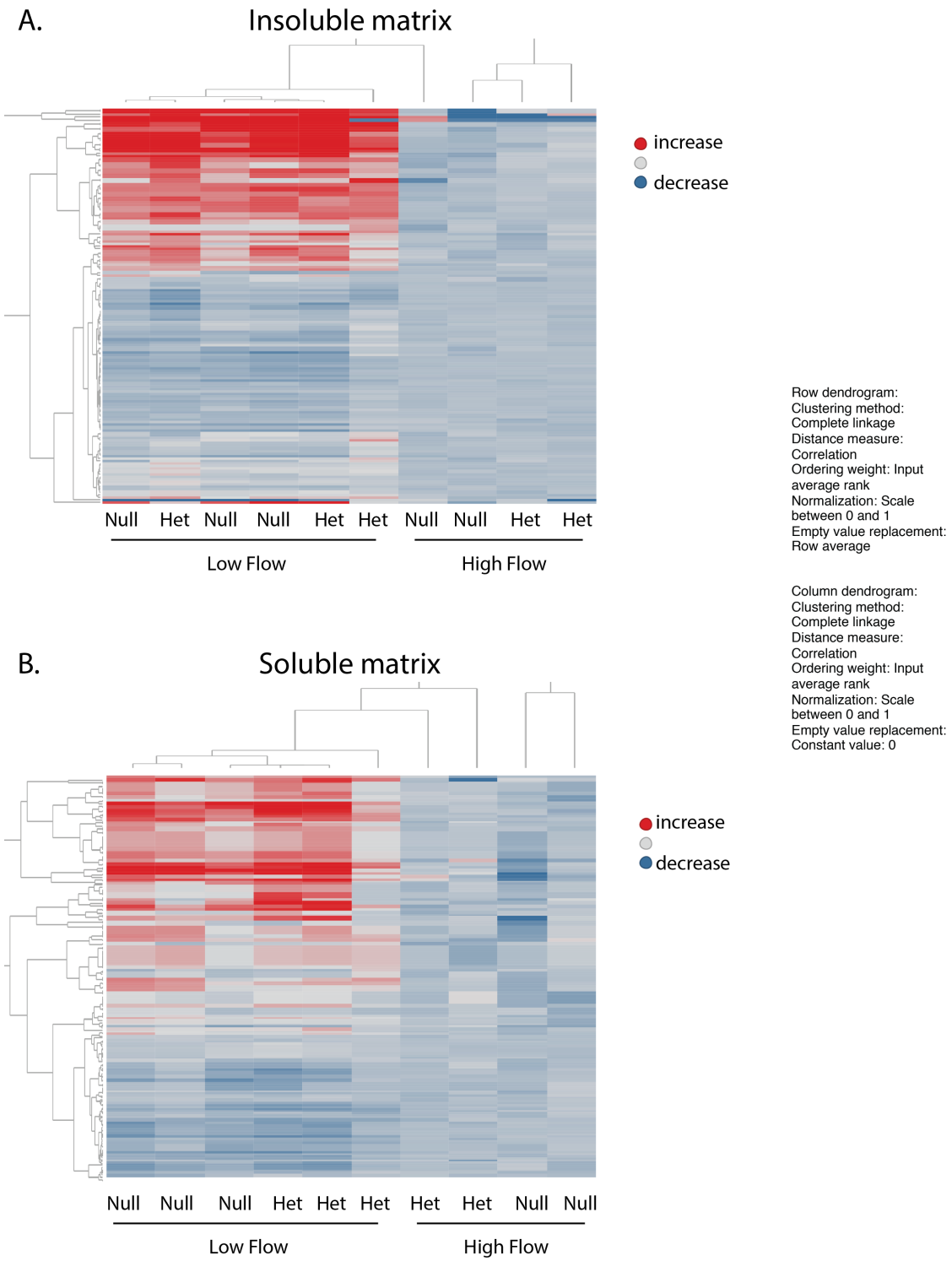

SI Figure 4. Heat map showing clustering of matrisome changes between pools of carotid arteries. Figure shows clustering of proteins (rows) by increase or decrease (in Log2 fold-change) relative to average high flow artery pools for both insoluble (A) and soluble (B) proteins. Clustering is complete linkage by correlation. The scale bar is set so that graded with a maximum at Log2 fold-change 3 increase (red) or minimum at Log2 fold-change -3 decrease (blue).

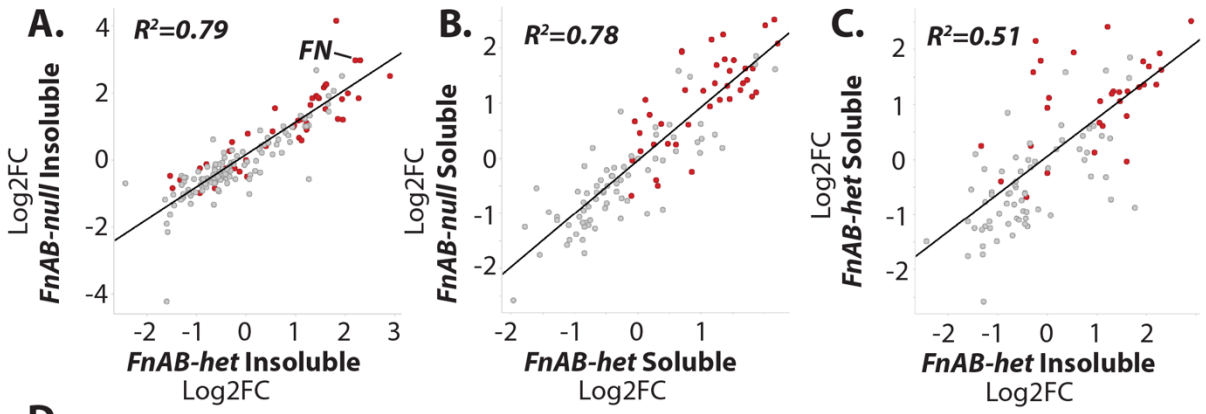

D.

Gene ID	Insoluble *Log2FC* Het	Insoluble *Log2FC* Null	Insoluble *Log2FC* #Pep	Soluble *Log2FC* Het	Soluble *Log2FC* Null	Soluble *Log2FC* #Pep
IGHG1	1.8	4.2	1	n.d.	n.d.	n.d.
FGG	2.9	2.5	7	2.5	2.2	10
SERPINB1A	1.9	2.5	2	n.d.	n.d.	n.d.
FN1	2.3	3.0	23	1.6	1.8	34
C4BPA	n.d.	n.d.	n.d.	2.1	2.2	1
CTGF	1.4	2.7	1	n.d.	n.d.	n.d.
IGKC	2.2	3.0	3	1.4	1.7	1
F2	1.6	2.2	2	n.d.	n.d.	n.d.
GC	n.d.	n.d.	n.d.	2.2	1.3	1
COL11A1	1.7	1.9	2	n.d.	n.d.	n.d.
MBL1	n.d.	n.d.	n.d.	1.7	1.9	1
PLG	1.9	1.8	2	1.8	1.5	2
FGB	2.0	2.0	9	1.7	1.2	13
PZP	1.7	1.4	3	1.8	1.9	14
IGHM	2.3	1.8	3	1.9	0.7	9
F13B	1.4	1.9	2	n.d.	n.d.	n.d.
APOH	n.d.	n.d.	n.d.	1.6	1.7	2
FGA	1.2	0.9	9	2.4	2.0	3
ITIH2	n.d.	n.d.	n.d.	1.4	1.7	1
FBLN2	1.2	1.2	7	1.6	2.2	3
ITIH1	1.3	1.8	5	1.2	1.6	3
C4B	1.3	1.6	3	1.2	1.9	3
CFH	1.6	2.3	6	1.2	0.7	3
APOA1	1.8	1.2	4	1.3	1.4	9
VTN	1.9	1.2	3	1.4	1.2	6
ITIH4	1.5	1.8	5	1.1	1.3	2
SERPINH1	1.7	1.7	4	1.5	0.8	3
MUG1	1.5	1.9	4	1.2	1.0	3
TF	n.d.	n.d.	n.d.	1.1	1.5	20
C3	1.6	2.2	17	0.8	0.2	15
C8A	1.2	1.1	1	n.d.	n.d.	n.d.
SERPINF2	1.1	1.2	1	n.d.	n.d.	n.d.
P4HA1	1.2	1.0	3	n.d.	n.d.	n.d.
LEPRE1	1.2	1.0	1	n.d.	n.d.	n.d.
FBLN1	0.6	1.5	1	n.d.	n.d.	n.d.
AHSG	0.0	0.0	0	0.9	1.1	1
ECM1	1.1	1.3	4	0.4	1.2	3
F13A1	0.5	0.9	2	1.9	0.7	3
IGH-3	1.0	1.0	1	n.d.	n.d.	n.d.
TTR	0.0	0.8	1	1.1	1.8	2
LTBP2	0.7	1.0	2	0.0	0.0	0
ALB	-0.3	0.5	11	1.6	1.4	31
TNC	1.3	1.0	8	0.4	0.6	5
CLU	1.1	0.6	6	0.6	0.8	5
COL12A1	0.4	0.5	6	1.6	0.6	1
ANXA2	0.9	1.0	9	0.6	0.5	6
APOE	1.6	1.5	4	0.0	-0.1	1
APOA4	1.1	0.7	3	1.1	0.1	1
THBS1	1.0	1.2	7	0.7	0.0	7
C5	-0.2	-0.3	1	2.2	1.2	3
COL14A1	0.3	0.9	15	0.6	1.0	14
ANXA1	0.6	0.6	8	0.2	1.3	4
HPX	-0.1	-0.4	2	1.8	1.4	10
CTSD	0.8	0.7	2	0.6	0.3	1
POSTN	0.8	0.8	13	0.1	0.6	14
COL6A3	1.8	2.1	1	-0.9	-0.8	36
PLXNB2	0.4	0.7	2	n.d.	n.d.	n.d.
VWA5A	0.6	0.5	2	n.d.	n.d.	n.d.
APOA2	0.9	1.0	1	0.1	0.0	1
NID1	0.3	0.4	5	0.4	1.0	3
SERPINF1	n.d.	n.d.	n.d.	0.6	0.4	1
SERPINB9	0.5	0.5	3	n.d.	n.d.	n.d.
LMAN1	1.2	1.2	2	-0.3	-0.4	1
LGALS1	0.7	0.2	4	0.4	0.3	4
COL8A1	1.3	1.3	1	-0.7	-0.3	2
APOB	0.4	0.4	1	n.d.	n.d.	n.d.
CPN2	n.d.	n.d.	n.d.	0.3	0.5	1
LAMB1	0.5	0.2	3	n.d.	n.d.	n.d.
COL23A1	1.3	-0.6	1	n.d.	n.d.	n.d.
ORM1	0.0	0.0	0	-0.2	0.9	1
PRG2	0.3	0.3	1	n.d.	n.d.	n.d.
HCFC1	0.3	0.2	1	n.d.	n.d.	n.d.
SERPINA1E	n.d.	n.d.	n.d.	0.5	0.0	1
TGFBI	0.9	0.5	6	-0.3	-0.1	5
AEBP1	-0.3	-0.2	9	0.3	0.9	3
GSN	-0.3	0.3	10	0.2	0.2	6
THBS3	-0.1	0.2	1	n.d.	n.d.	n.d.
SERPINB6A	0.2	0.0	1	n.d.	n.d.	n.d.
IGFBP7	-0.2	-0.1	4	0.0	0.4	4
SERPINE2	-0.3	0.3	4	n.d.	n.d.	n.d.
S100A11	-0.7	0.6	1	n.d.	n.d.	n.d.
ANGPTL2	0.3	-0.4	1	n.d.	n.d.	n.d.
SERPINA1D	n.d.	n.d.	n.d.	-0.5	0.3	2
HTRA3	0.0	-0.2	1	n.d.	n.d.	n.d.
EMILIN1	0.0	-0.1	13	-0.2	-0.2	4
S100A4	0.2	-0.3	2	0.2	-0.7	2
COL5A3	-0.3	-0.1	3	n.d.	n.d.	n.d.
PXDN	0.1	-0.5	2	n.d.	n.d.	n.d.
EMILIN2	-0.3	-0.1	2	n.d.	n.d.	n.d.
CSPG4	-0.4	-0.7	4	0.0	0.3	3
GPX3	0.0	-0.5	4	n.d.	n.d.	n.d.
SERPINB6B	0.1	-0.6	1	n.d.	n.d.	n.d.
LAMA5	-0.8	-0.8	15	0.9	-0.3	3
ADIPOQ	-1.3	-0.6	2	0.2	0.6	3
ELN	-0.4	0.2	7	-0.6	-0.3	3
COL4A3	-0.5	-0.1	1	n.d.	n.d.	n.d.
LAMC1	-0.6	-0.6	24	0.0	-0.1	9
ANXA3	-0.3	-0.3	4	n.d.	n.d.	n.d.
SERPINC1	-0.9	-0.3	3	-0.4	0.3	4
HSPG2	-0.5	-0.3	37	-0.9	0.4	38
LGALS9	-0.4	-0.3	1	n.d.	n.d.	n.d.
COLEC12	-0.5	-0.1	5	n.d.	n.d.	n.d.
NID2	n.d.	n.d.	n.d.	-0.3	-0.4	4
LUM	-0.4	-0.3	10	-0.7	-0.1	10
BGN	-0.2	0.1	3	-0.9	-0.5	11
CTSZ	-0.6	-0.1	2	n.d.	n.d.	n.d.
FGL2	-0.2	-0.6	1	n.d.	n.d.	n.d.
COL4A2	-0.6	-0.3	12	-0.4	-0.3	3
ANXA6	-0.5	-0.4	10.0	-0.2	-0.5	6
CTSH	-0.4	-0.4	1	n.d.	n.d.	n.d.
LAMA4	-0.9	-0.7	8	-0.2	0.2	4
NPNT	-1.4	-1.4	5	0.1	1.0	2
ZFR	-0.4	-0.5	1	n.d.	n.d.	n.d.
ANXA7	-0.3	-0.5	4	-0.1	-0.8	1
HTRA1	0.1	-1.0	1	-1.0	0.1	2
CP	-0.8	-0.1	1	n.d.	n.d.	n.d.
MGP	n.d.	n.d.	n.d.	-0.5	-0.5	1
LTBP1	-0.6	-0.2	6	-0.5	-0.6	2
MFAP5	-0.5	-0.6	1	n.d.	n.d.	n.d.
FBN1	-0.5	-0.5	19	-0.6	-0.6	8
TGM2	-0.6	-0.7	7	-0.4	-0.6	5
COL1A2	-0.4	0.1	112	-1.1	-0.9	35
ANXA5	-0.6	-0.5	8	-1.1	-0.3	8
COL18A1	-0.7	-0.5	10	-0.8	-0.5	11
EFEMP1	-0.8	-0.5	4	-0.6	-0.5	3
ASPN	-0.5	-0.6	3	-0.7	-0.7	8
S100A6	-0.4	-0.4	2	-0.9	-0.8	2
LOX	-0.6	-1.3	2	-0.5	-0.3	1
EFEMP2	-1.3	-0.7	1	-0.8	-0.2	2
ANXA4	-0.9	-0.6	3	n.d.	n.d.	n.d.
COL5A1	-0.8	-0.6	15	-0.6	-0.9	3
LAMA2	-0.9	-0.6	2	n.d.	n.d.	n.d.
PRELP	-0.4	-0.5	7	-1.2	-0.9	11
THSD4	-0.6	-0.9	1	n.d.	n.d.	n.d.
LTBP4	-1.3	-1.1	6	-0.2	-0.4	6.0
CFI	-0.6	-0.8	1	n.d.	n.d.	n.d.
PCOLCE	-0.5	-0.9	1	n.d.	n.d.	n.d.
COL1A1	-0.8	-0.2	168	-1.2	-0.8	54
LAMB2	-0.8	-0.7	14	-0.8	-0.9	5
PLXDC2	-1.0	-0.6	1	n.d.	n.d.	n.d.
COL6A2	-0.4	-0.5	23	-1.2	-1.1	9
COL2A1	-1.2	-0.5	17	n.d.	n.d.	n.d.
MFGE8	-1.1	-1.3	3	-0.6	-0.5	5
COL4A4	-0.9	-0.9	1	n.d.	n.d.	n.d.
COL15A1	-1.1	-1.1	4	-0.6	-0.8	5
COL6A1	-0.6	-0.7	16	-1.1	-1.3	11
COL5A2	-1.0	-0.4	27	-1.0	-1.4	4
ANXA11	-0.7	-0.7	4	-1.4	-1.0	1
COL4A1	-1.2	-0.5	6	-1.2	-0.8	1
SERPING1	-0.9	-1.0	1	n.d.	n.d.	n.d.
TNXB	-1.2	-0.9	14	-1.1	-0.8	3
VWF	-1.5	-0.5	1	n.d.	n.d.	n.d.
OGN	-1.1	-1.0	5	-1.2	-0.8	4
COL3A1	-1.3	-0.5	110	-1.7	-0.8	37
DCN	-1.0	-1.0	9	-1.5	-0.9	10
VCAN	-1.3	-1.2	3	-1.3	-0.7	2
COL4A6	-1.3	-1.0	6	n.d.	n.d.	n.d.
C1QA	-1.5	-0.9	1	n.d.	n.d.	n.d.
FBLN5	-1.3	-0.7	3	-1.6	-1.1	5
ABI3BP	-1.5	-1.6	3	-0.5	-1.6	2
TINAGL1	-1.5	-1.1	2	-1.2	-1.8	1
COL4A5	-1.6	-1.2	2	n.d.	n.d.	n.d.
DPT	-2.4	-0.7	2	-1.5	-1.1	1
MFAP4	-1.6	-1.9	3	-1.7	-1.5	4
COL6A6	-1.3	-1.1	7	-2.6	-2.0	1
MFAP2	-1.6	-2.1	1	n.d.	n.d.	n.d.
PRSS1	-1.6	-4.2	2	-1.1	-1.3	4

SI Figure 5. Matrisome composition under low and disturbed flow

Plots showing the correlation between the regulation of matrisome and blood-derived protein levels under low flow between *FnAB-het* and *FnAB-null* mice in the (A) insoluble fraction, and (B) the soluble extracellular fraction. X and Y axis are Log2 fold-change (low flow artery vs high flow artery). All points shown represent a single protein with at least two peptides, and points in red mark proteins that are abundant in blood. (C) Plot showing the correlation between soluble and insoluble fractions in the same response in *FnAB-het* mice. (D) Table of all protein changes, average Log2 fold-change under low-flow conditions, including both soluble and insoluble fractions, is indicated with the bar (blue increased and red decreased under low flow; blood proteins labelled in red text). Log2 fold-changes (Log2FC) for the indicated genotypes in the specified matrisome fraction (soluble or insoluble) are shown, along with the number of peptides used. "n.d."=not detected.

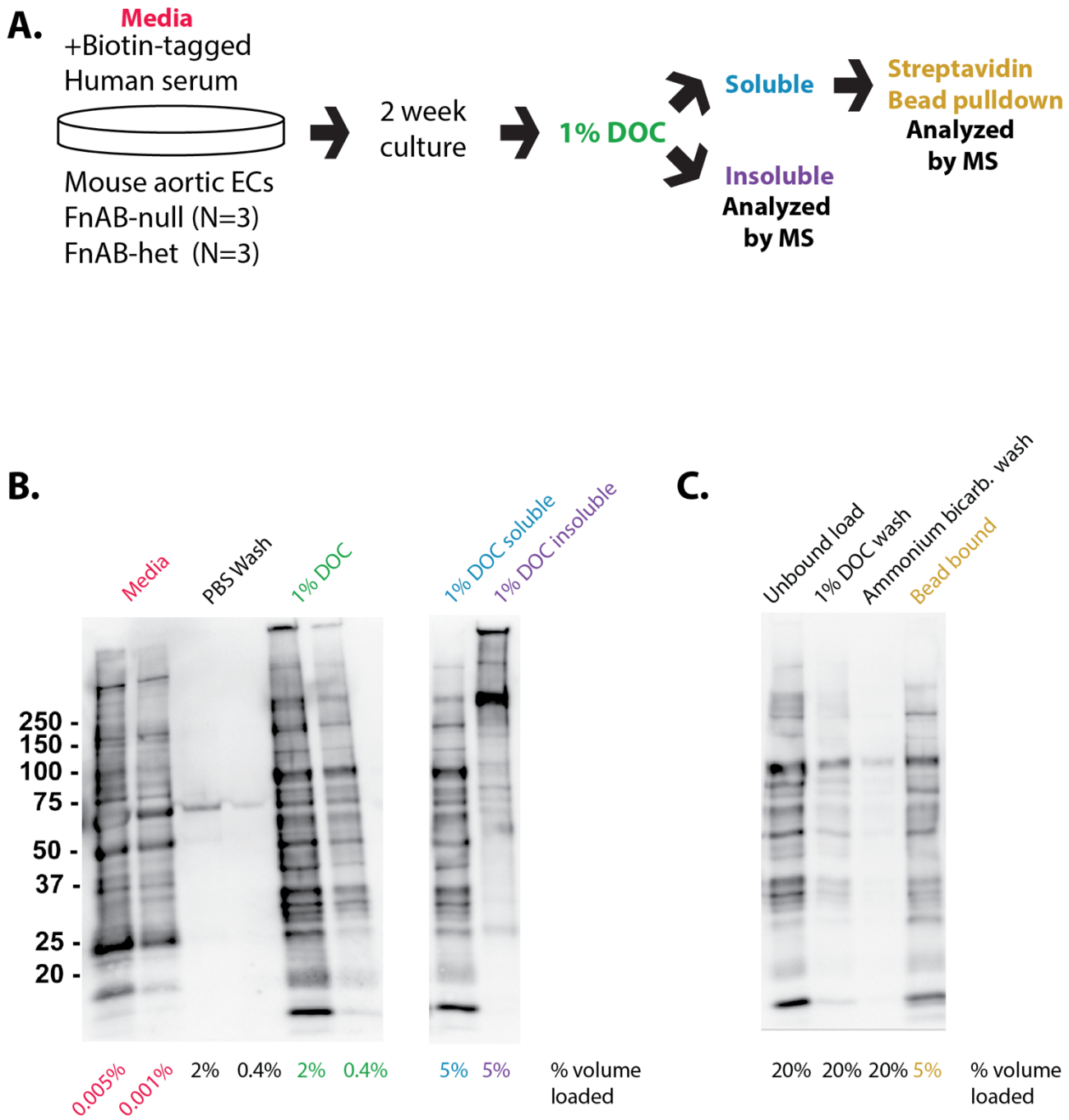

SI Figure 6. Enrichment of biotin bound proteins in the 1% DOC soluble and insoluble fractions of aortic endothelial cells.

(A) Outline of the experiment. Cells were allowed to attach and grow in 10% human serum in DMEM medium spiked with biotin-tagged human serum. After two weeks of culture, media was spiked again and cells and matrix were resuspended in 1% DOC. This was assessed directly, relative to the media by streptavidin western blots (B). Then, 1% DOC was separated into 1%DOC soluble and 1%DOC insoluble by centrifugation, and similarly assessed by western blot (B). Finally, extracellular proteins from the 1%DOC soluble fraction were isolated by binding to neutravidin beads, and the starting material as well as washes and final bead bound protein were analyzed by streptavidin western blot (C). For each of these fractions, the % of the total fraction which was loaded on the gel is shown.

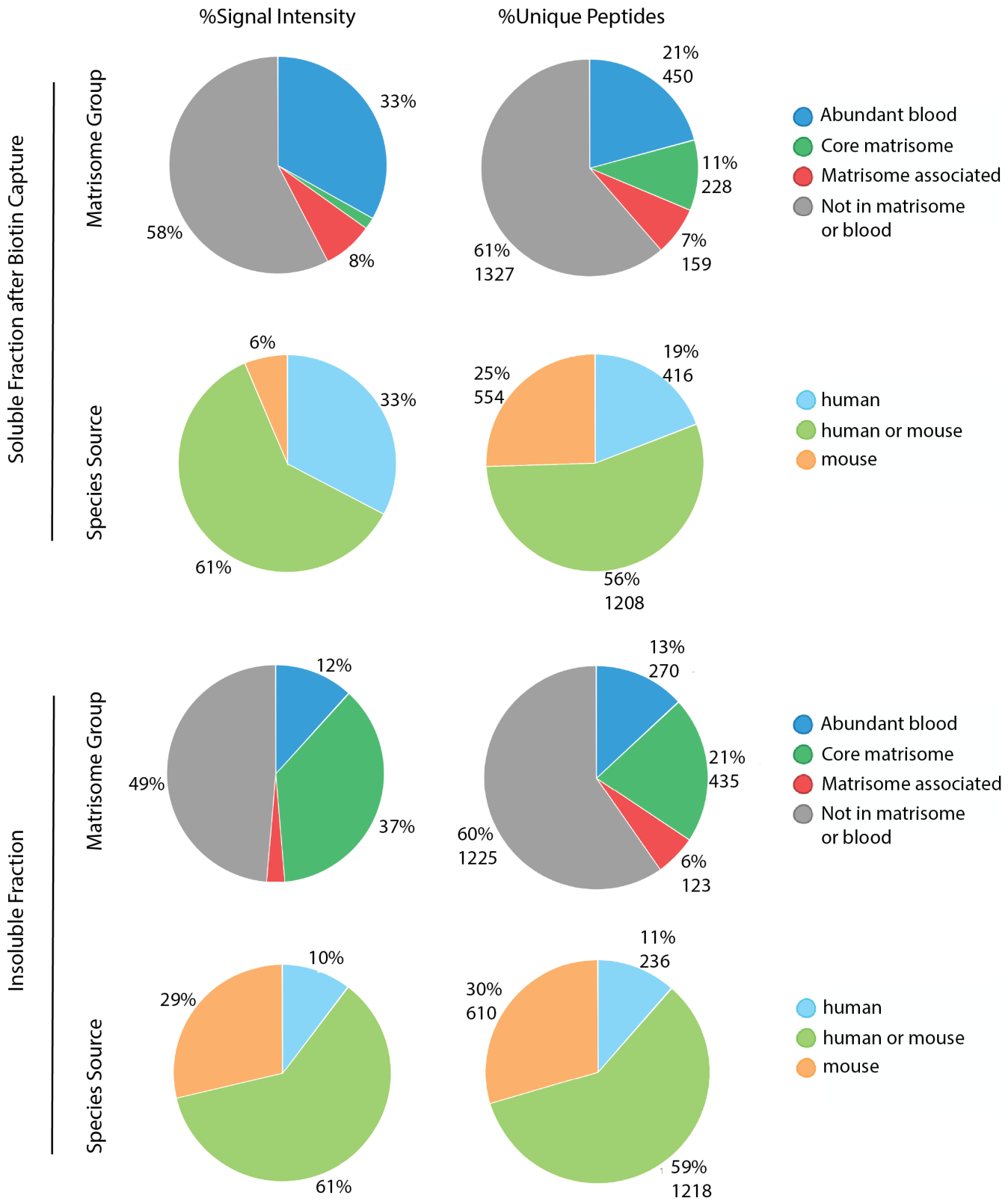

SI Figure 7. Unique Peptides and Signal Intensity from Soluble and Insoluble Fractions *in vitro*
Pie charts show percentage of signal intensity and percentage of unique peptides that were attributed to each of the indicated groups.

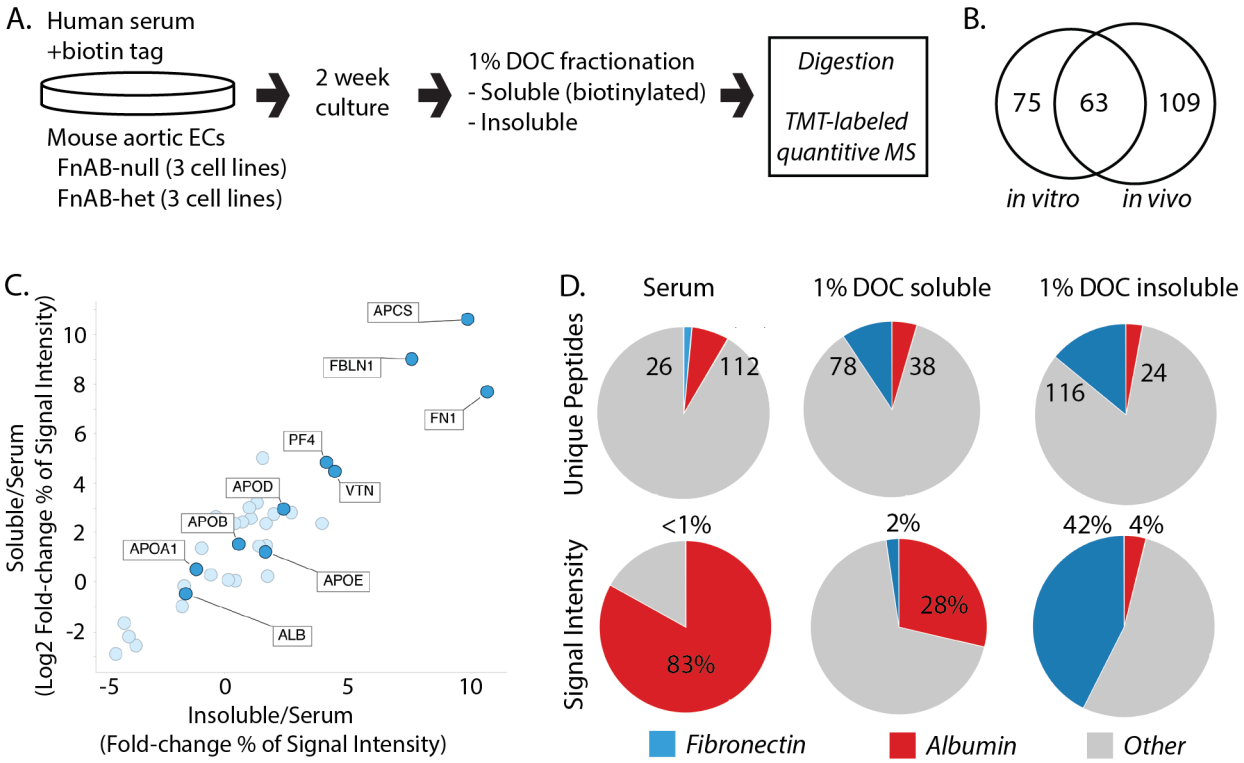

SI Figure 8. Biotin-tagging of serum proteins reveals selective deposition into the matrisome *in vitro*. (A) Schematic of methods for the enrichment of arterial matrisome from *FnAB-null* and *FnAB-het* cells. At 2 weeks, the cellular monolayer was extensively washed with PBS, and solubilized in 1% DOC. Insoluble proteins were identified in the 1% DOC-insoluble fraction, Soluble proteins were extracted from the 1% DOC fraction by their biotin tags using streptavidin beads. (B) Overlap among the matrisome and blood proteins identified by mass spectrometry from carotid arteries *in vivo* and from endothelium *in vitro*. (C) Change in the proportion of signal intensity in the top human serum proteins in the soluble and insoluble fractions relative to their original serum sample. Positive values indicate an enrichment relative to the serum sample (e.g. FBLN1 and FN1), and negative values indicate disenrichment (e.g. ALB). X and Y axis represent Log2 fold-change in the % of total ion-signal intensity attributed to the specific protein of interest over the % of total ion-signal intensity attributed to that same protein in serum (e.g. 5% of ion-signal intensity for FN in the insoluble matrix vs 0.5% in serum is a 10 fold change). (D) % of ion signal derived from albumin and fibronectin in the indicated fractions, among all human peptides identified.

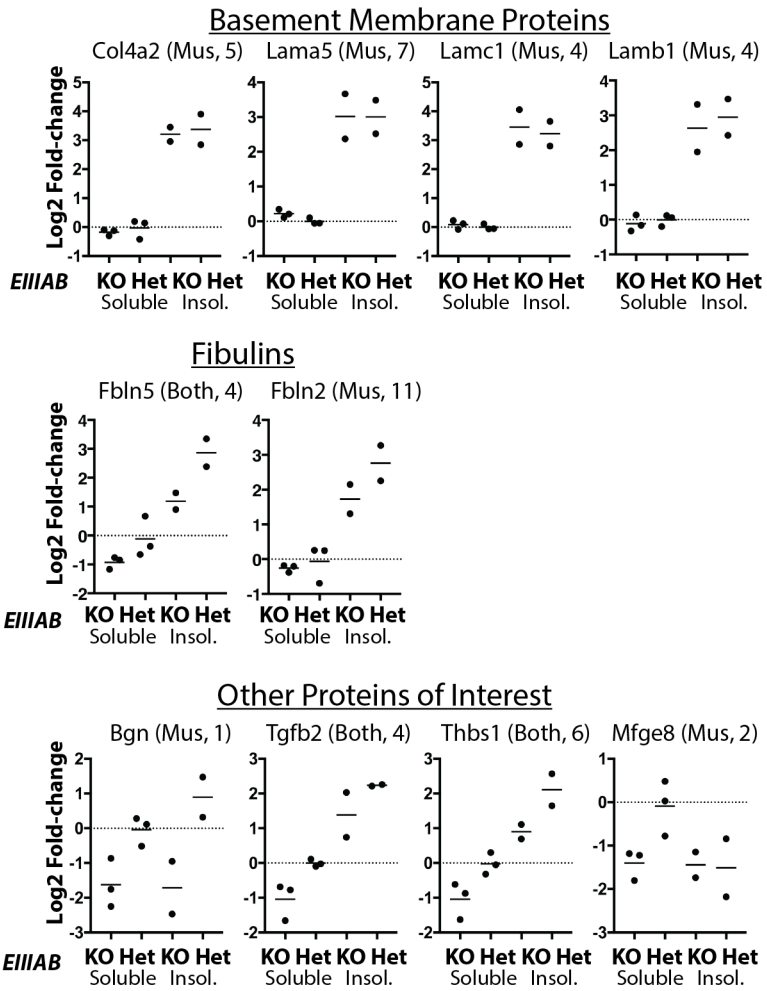

SI Figure 9. Proteins differentially bound into soluble and insoluble fractions of *FnAB-null* and *FnAB-het* cells *in vitro.* Each point is a biological replicate from a separate immortalized aortic cell line from littermate mice (N=3 *FnAB-null* and N=3 *FnAB-het*). Only four of the six insoluble fractions were assessed. Mus=mouse specific peptide identification, H.Sp.=human specific peptide identification, Both=ambiguous, human or mouse.

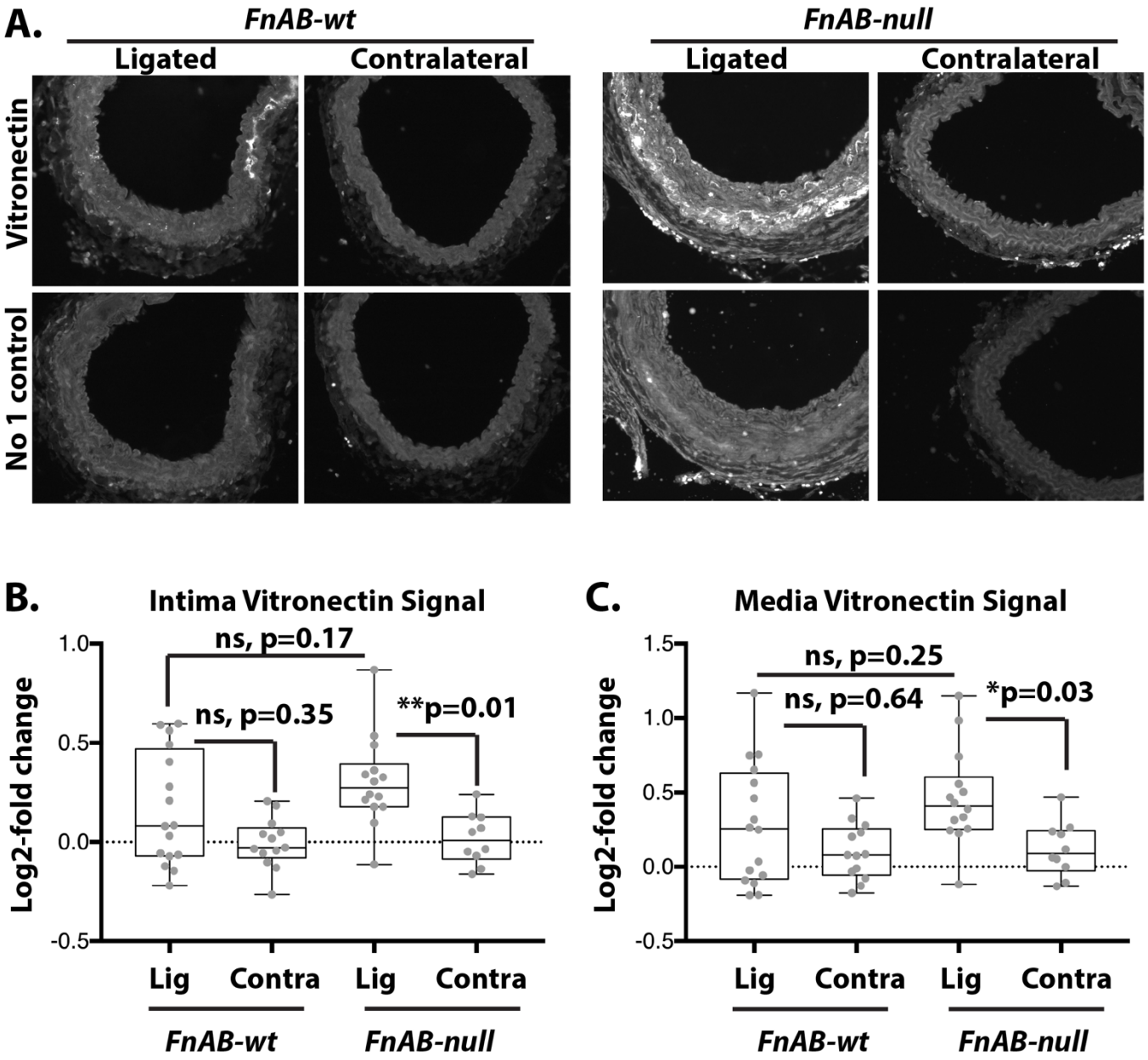

SI Figure 10. Vitronectin deposition in intima and media under low and disturbed flow .
(A) Immunofluorescence staining for Vitronectin, with no primary antibody controls for the indicated genotypes and arteries. Signal is light against a dark background. (B&C) Quantitation of antibody staining intensity performed in ImageJ, with automated selection of intimal (B) and medial (C) layers. Each point in B and C is an average of between 1 and 3 sections from an individual animal of the indicated genotypes. Statistical analysis is by Kruskal-Wallis with Dunn's post-hoc comparisons.

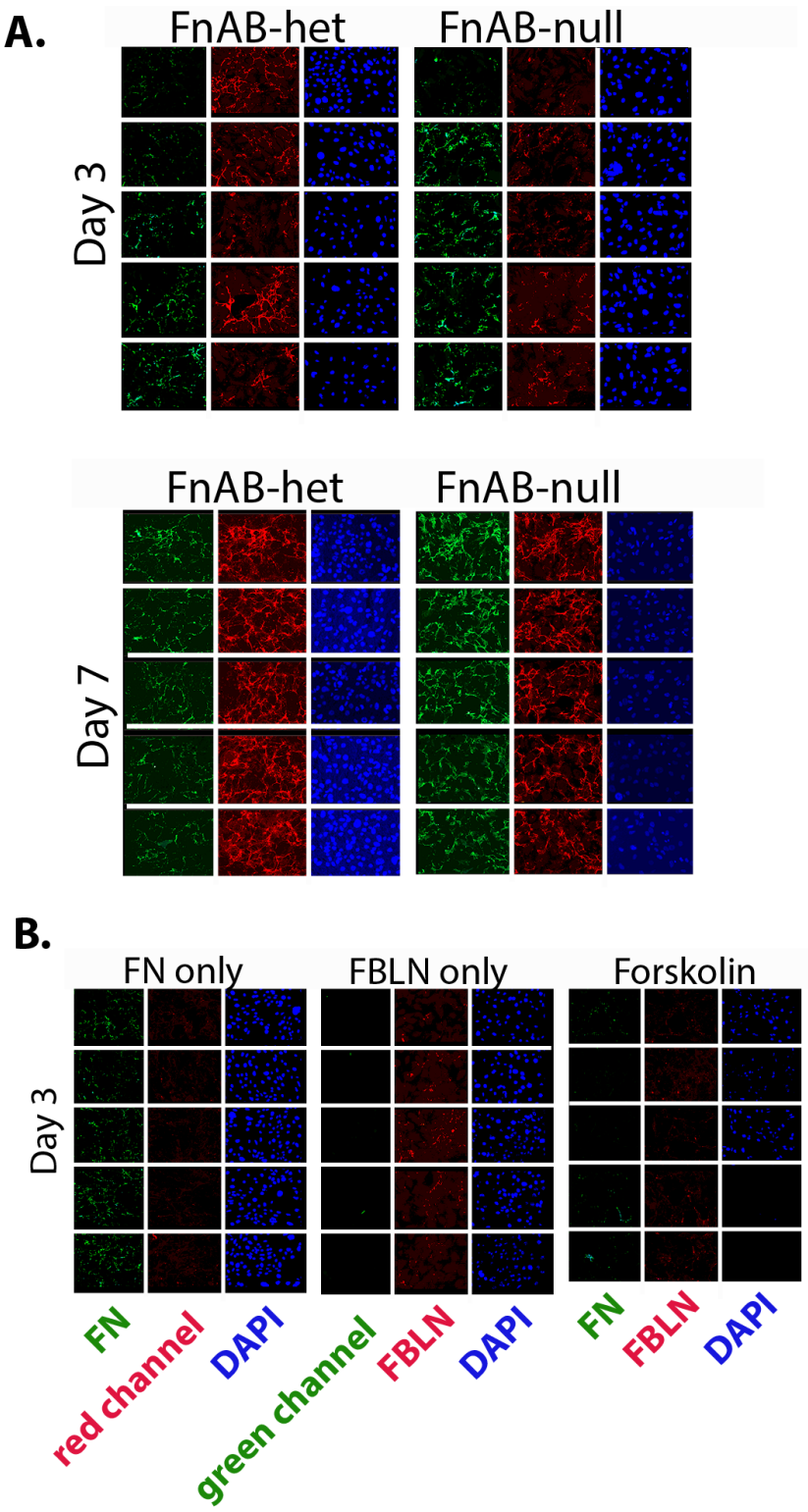

SI Figure 11. Fluorescence images of FBLN1 and FN in cultured endothelial monolayers
(A) Immunofluorescence staining of cultured aortic endothelial cells from FnAB-het or FnAB-null mice, panels show FN, FBLN and DAPI separately from the same location (left to right). Fluorescence was adjusted independently at each timepoint (but equivalently between het and null) to show fibrils. (B) Control staining with single antibodies or of cells with impaired FN deposition by forskolin treatment.

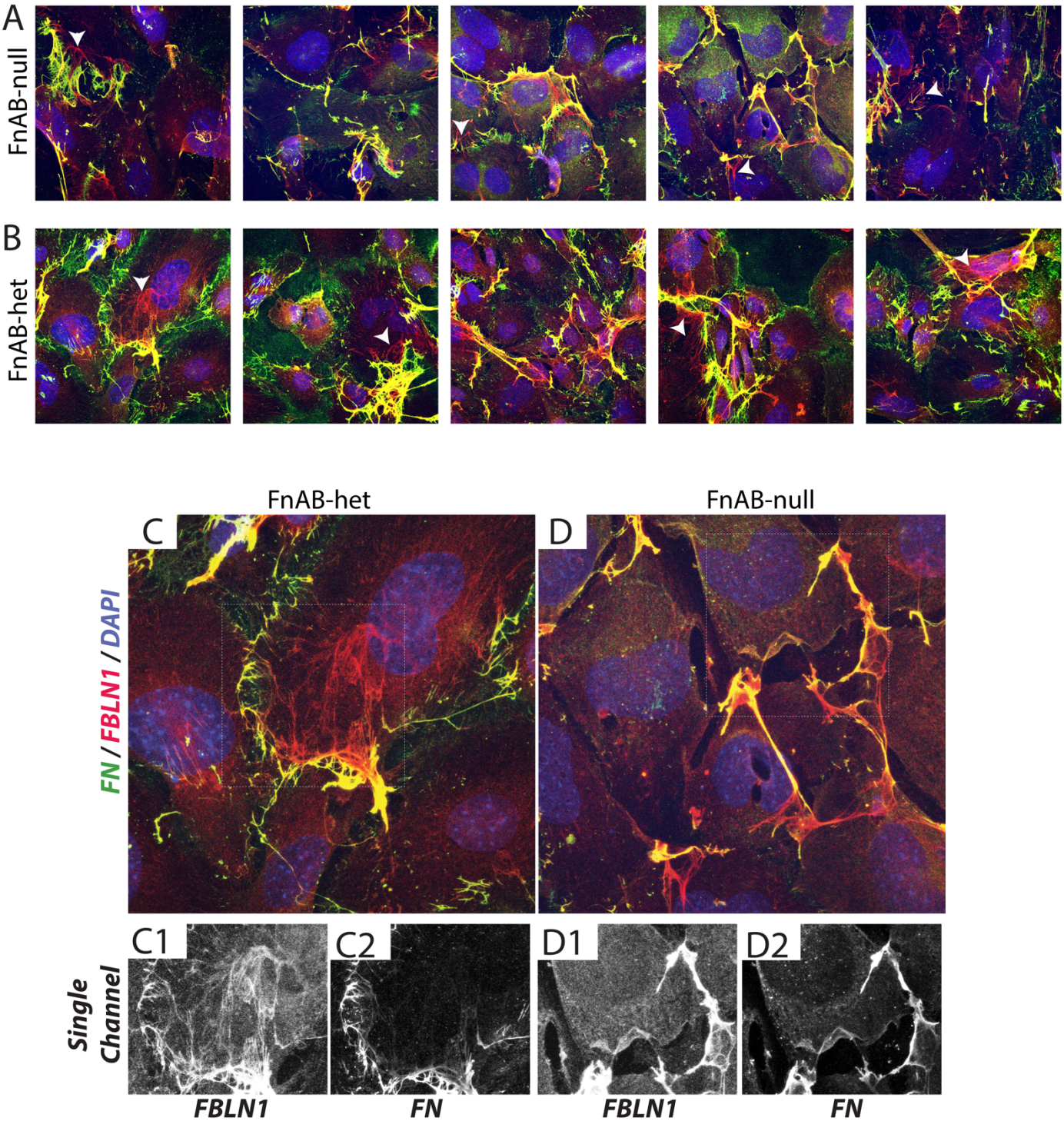

SI Figure 12. High-magnification Fluorescence images of FBLN1 and FN in cultured endothelial monolayers. (A-D) Immunofluorescence staining of cultured aortic endothelial cells from FnAB-het (B,C) or FnAB-null (A,D) mice, panels showing overlay of FN (green), FBLN (red) and DAPI (blue). White arrowheads point at regions where FBLN1 expression extends beyond detectable FN fibrils. C and D are higher magnfications of panels above, showing individual FBLN1 (C1 and D1) and FN (C2 and D2) channels.

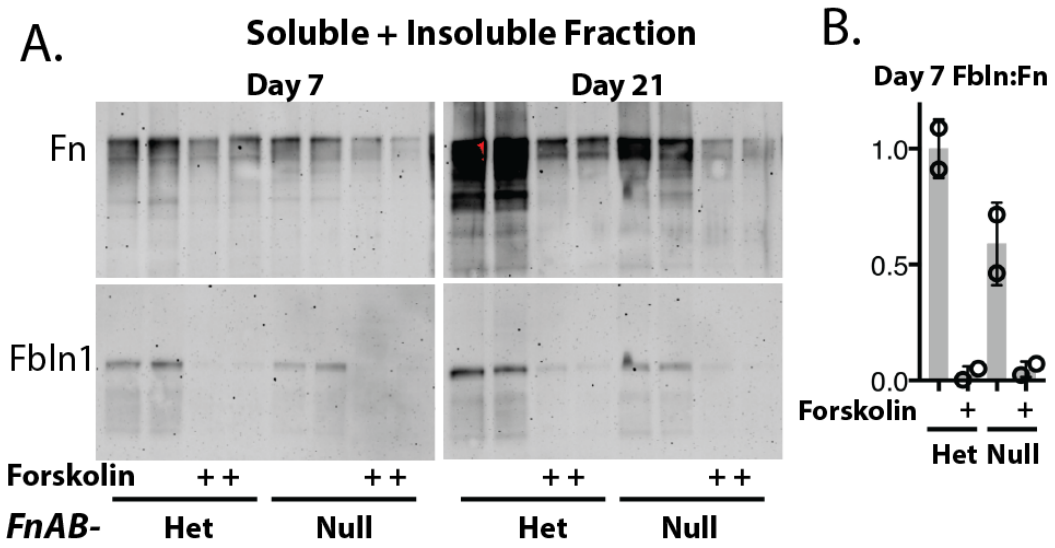

SI Figure 13. Deposition ratio of FBLN1 and FN is consistent over time, and is blocked by forskolin
(A) Western blots and (B) quantitation showing total Fibulin-1 and Fibronectin from a pair of *FnAB-null* and *FnAB-het* cells in culture with human serum, with and without Forskolin treatment to block fibrillogenesis.